LASER BASED ULTRASONICS FOR DEFECT CHARACTERIZATION IN COMPOSITE MATERIALS
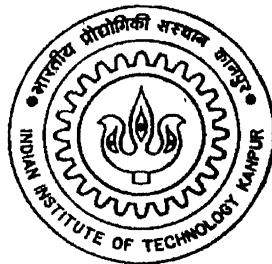
By

Nitin Khanna
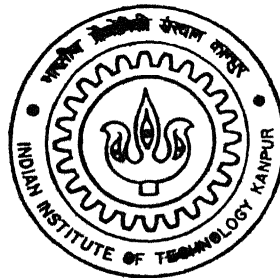
LASER BASED ULTRASONICS FOR DEFECT CHARACTERIZATION IN COMPOSITE MATERIALS

A Thesis Submitted

in Partial Fulfillment of the Requirements

for the Degree of

MASTER OF TECHNOLOGY

by

NITIN KHANNA

to the

MATERIAL SCIENCE PROGRAMME

INDIAN INSTITUTE OF TECHNOLOGY, KANPUR

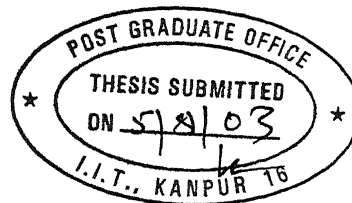JULY, 2003

CERTIFICATE

It is certified that the work contained in the thesis entitled " **Laser Based Ultrasonics for defect characterization in composite materials**" by Mr. Nitin Khanna has been carried out under our supervision and that this work has not been submitted elsewhere for a degree

(Dr. K. K. Kar)

(Asst. Professor)

Material Science Programme

Indian Institute of Technology, Kanpur.

(Dr. P. Munshi)

(Professor)

Department of Mechanical Engineering

Indian Institute of Technology, Kanpur.

July, 2003

DEDICATED

TO

MY BELOVED PARENTS

ACKNOWLEDGEMENTS

ABSTRACT

Non-Destructive Evaluation (NDE) involves the characterization of material properties and/or defects without detrimental effects on the structure examined. NDE can be performed using ultrasound, x-rays, microwaves or magnetic flux. Ultrasound has a wide range of applicability in performing NDE of materials and structures. In Ultrasonic Non-Destructive Testing and Evaluation, use is made of the properties of elastic waves propagation in solids in order to detect the defects and materials inhomogeneties. In Ultrasonic NDE, the different features of ultrasonic waves, namely frequency, amplitude, time of flight etc can be used for detection and sizing of internal defects. Ultrasonic Tomography (UT) is used to characterize a defect or inhomogeneity by Time of Flight (TOF) information. The accuracy of reconstruction depends on the correctness of TOF determination and also on the specific algorithm used.

The present work is on the use of TOF measurement and subsequent image reconstruction. In this study, the thermo-elastic waves induced in glass/epoxy composites with metal inserts by Laser Based Ultrasonics (LBU) are considered. The Time of Flight has been used for tomographic reconstruction of a specimen having defect using Algebraic Reconstruction Technique (ART) and Multiplicative Reconstruction Technique (MART) algorithms. The Tomographic reconstructions using different values of relaxation parameter and initial guess have been used to discuss the nature and suitability of these algorithms for defect reconstruction. Finally, Simulation study is conducted to check the performance of various algorithms and review the experimental results.

CONTENTS

List of Figures

LIST OF TABLES

Chapter 1

INTRODUCTION

1.1 INTRODUCTION

The present work on the identification and reconstruction of defects in composite materials requires a thorough understanding of behavior of composite materials, ultrasonic wave propagation and analysis from experimental and theoretical viewpoint A brief introduction to related topics is given below

Demands imposed by modern advanced technologies on materials have become so diverse and severe that single component conventional materials often cannot meet them It is necessary to combine two or more materials to make a composite to meet the demands Constituents not only contribute their respective share, but their action transcends the sum of the individual properties and provides new performance unattainable by constituents acting alone Composites can be formally defined as materials having two or more chemically distinct constituent materials or phases with clear interfaces on a macro scale between them

The fiber reinforced materials are probably the most important class of composite materials which are widely used in structural applications particularly when weight saving is crucial These materials offer high strength-to-weight and modulus-to-weight ratios apart from their properties of excellent corrosion resistance, formability and mechanical properties, which can be controlled to a significant degree

Non-destructive testing (NDT) may be defined as the science of examining objects, materials or systems, in order to determine their fitness for certain purposes, without impairing their future usefulness or their desirable properties The term is generally applied to non-medical investigations of material integrity Non-destructive evaluation (NDE) of material plays a vital role in quality assurance of structural members during

manufacturing stage and operating life In general, the various NDE techniques can be placed into two categories active and passive The active techniques are those where something is introduced into or onto the specimen and a response is expected if a defect is present where as passive techniques are those that monitor or observe the item during either a typical load environment or a proof cycle and attempt to determine the presence of a defect through reaction of specimen Magnetics, ultrasonics, radiography fall in the category of active NDE and acoustic emission, noise analysis, leak testing etc are the examples of passive NDE Being one of the most commonly used non-destructive testing (NDT) methods, ultrasonic testing (UT) is rapidly developing in recent years

Ultrasonic inspection involves impinging a low energy, high frequency stress pulse into the material under inspection and examining the subsequent propagation of this energy It not only detects bulk and surface flaws, but also obtains information on material microstructure to determine engineering properties, such as elastic moduli and ultimate tensile strength However, traditional ultrasound requires liquid or contact coupling for its transmission, making it difficult or impossible to apply in many industrial situations This occurs in particular on curved parts and on parts at elevated temperature, a situation widely found in industrial products and during the processing of industrial materials

In conventional method, a piezoelectric transducer (or probe) generates ultrasonic waves, which propagate in the elastic medium and are detected either by the same (pulse-echo) or by a different transducer (through transmission) Although piezoelectric transducers are commonly used for non-destructive testing, several problems are associated with the requirement that they have to be bonded to the test material with an acoustical impedance matching coupling medium For velocity measurements, which are necessary for material thickness measurements and to locate the depth of defects, the coupling medium can cause transit time errors Due to the partial transmission and partial reflection of the ultrasonic energy in the couplant layers, there may be a change of shape of the waveform, which can further affect the accuracy of the velocity measurement This can also lead to serious errors in absolute attenuation measurements, which is the reason that so few reliable absolute measurements of attenuation are reported in the scientific literature Therefore, a method of non-contact generation and detection of ultrasound is of great

practical importance Several such techniques are presently available in various stages of development, namely capacitive pick-ups, electromagnetic acoustic transducers (EMATS), laser beam optical generators and detectors, and more recently air (or gas) – coupled ultrasonic systems However, as the name implies, capacitive pick-ups cannot be used as ultrasonic generators and, even when used as detectors, the air gap required between the pick-up and test structure surface is extremely small, which in essence causes the device to be very nearly a contact one The problem with EMATS is that the efficiency of ultrasound generation and detection rapidly decreases with lift-off distance between the EMATS face and the surface of the test object They can obviously be used only for examination of electrically conductive materials Because of the physical processes involved they are much better detectors than generators of ultrasound Laser-based ultrasound (LBU) generation and detection overcomes all of these problems and make truly non-contact ultrasonic measurements in both electrically conductive and non-conductive materials, in materials at elevated temperatures, in corrosive and other hostile environments, in geometrically difficult to reach locations, and do all of these at relatively large distances from the test object surface Furthermore, lasers are able to produce simultaneously shear and longitudinal bulk wave modes, as well as Rayleigh and Lamb wave modes LBU system uses a pulsed laser to generate ultrasound and a continuous wave (CW) laser interferometer to detect the ultrasound at the point of interrogation to perform ultrasonic inspection Some of the important areas of application of LBU are

- Medical field
- Microwave electronics
- Defect identification in a wide range of materials, including metals concrete, ceramics and composites etc
- Aerospace industry
- Steel industry
- Nuclear reactors
- Microstructure analysis of ferrous and non-ferrous materials

An additional benefit of laser techniques is that they are capable of a high degree of absolute accuracy, since measurements can in principle be calibrated against the

wavelength of light There may be sensitivity penalties for using lasers rather than piezoelectric transducers or probes, and certainly they are likely to be more costly and complex to use Nevertheless they are beginning to make a small but significant impact in a limited number of applications where their benefits over other probes outweigh their disadvantages

Historically, investigators have used the terminology A-, B- or C-scan to describe the type of data taken during ultrasonic study of specimens An A-scan indicates a variation of signal amplitude with time, where the ordinate of the oscilloscope trace is proportional to the amplitude and abscissa to the time elapsed A B-scan is the presentation of data in the form of a depth profile versus position along a specimen A C-scan is the presentation of variation of any feature or feature set as a function of position of transducer in two dimensions relative to the surface of the examined specimen Essentially, the feature or feature set, used to construct C-scan image is extracted from the received ultrasonic waveform obtained in the A-scan mode Another recent way of representing ultrasonic data is by using tomographic technique which reconstructs a slice of an object from multiple projections Thus, tomography, if perfected, can provide better results

1.2 LITERATURE SURVEY

Non-destructive evaluation of advanced composite materials poses a challenge to researchers and applied technologists Ultrasonic methods, however, are most common and practiced widely because of the low cost, relative ease in their use and the amount of information that can be obtained from them In this section, an overall review of processing of ultrasonic signals to enhance the confidence of identification of defects in composite materials is presented

In ultrasonic techniques, information on defect characterization requires more evolved techniques than classical methods Modern non-destructive testing of materials has to provide the highest possible detection probability, the correct size and exact orientation of defects in the specimen The simplest acoustical characterizations of materials deal

with velocity measurements Some well-known techniques of calculating wave speed by measuring the time-of-flight are described in Krautkramer and Krautkramer [1]. Neslroth et al [2] introduced the idea of using various features of ultrasonic signal to detect various types of defects, flaws or anomalies in composite materials Rose [3] introduced a concept of feature mapping The basic concept is based on the fact that different types of defect are expected to interact distinctively with different features of ultrasonic signal He proposed the Fischer linear discriminant function as a classifier, which uses linear combination of useful features to detect anomalies Sarin [4] and Dahraju [5] have developed an experimental set-up using an Nd YAG pulsed laser for generation of ultrasound in specimens and a He-Ne continuous laser based heterodyne optical interferometric probe for detection of the same They have proposed a methodology for inspection of composite specimens using LBU and evaluation of effectiveness of different features of ultrasonic signals in detecting different types of defect Scruby and Drain [6] in their introductory book on this subject have elaborated on the principles underlying generation and reception processes of all techniques used

Tomographic imaging principles have been successfully applied to the problem of recovering local material properties from acoustic wave propagation data for many years While acoustic tomography has many features in common with its radiographic counterpart, there are additional complicating features (notably ray bending), which make tomography more difficult with acoustic data When anisotropy is included, the level of difficulty increases markedly Kline [7] used tomographic imaging principle to characterize the mechanical properties of anisotropic media His work is mainly focused on geophysical applications where weak anisotropy is assumed

Kline and Wang [8] developed a technique for ultrasonic tomography in anisotropic media The ART algorithm was modified, through the use of the governing equations for wave propagation in anisotropic media and composite micromechanics Variation of acoustic velocity with propagation direction is also taken into account Kline, Wang, Mignoga, and Delsanto [9] proposed an approach to ultrasonic tomography in anisotropic media based on finite difference formulation Chow, Hutchins, and Mottram [10]

conducted experiments in which acoustic emission and ultrasonic tomography were performed concurrently on samples of anisotropic glass fiber reinforced polymer composite in a direct tensile test Sullivan, Kline, and Mignona [11] developed an algorithm for acoustic tomographic reconstruction of fiber angle in orthotropic composites The fiber angle about the y-axis was constructed using a dimensional solution Rathore, Munshi, and Kishore [12] presented a new tomographic reconstruction method, C-ART, for anisotropic materials, which accounts for the directional dependence of sound velocity in the material Subbarao, Munshi and Muralidhar [13] studied the performance of ART, MART and MENT family of algorithms under limited data conditions Their study concludes that MART3 performs better than all other algorithms Farhan [14] made a brief study on ultrasonic tomography of Perspex/polystyrene composites, where the different acoustic impedances zones are clearly shown by using Convolution Back Projection algorithm

Ultrasonic measurements are widely used for the elastic constant determination of anisotropic materials Choosing an appropriate propagation direction and polarization, can maximize the accuracy of elastic constant measurement Six elastic constants for an orthotropic material can be determined from measurements along symmetry axes Degtyar and Rokhlin [15] proposed an inversion procedure based on nonlinear least square method to determine elastic constants from group or phase velocity data in orthotropic and transversely isotropic materials Bernard, Jenkins, and Wolfgang [16] developed a method, which optimally determines the elastic constants of anisotropic solids from wave-speed-measurements in arbitrary nonprincipal planes Reverdy and Audoin [17] describes a method for determining elastic constants of anisotropic materials from phase velocities of acoustic waves generated and detected by lasers Deschamps and Bescond [18] proposed a numerical method to recover the elastic constants from ultrasound group velocities

In the literature, only a few ray-tracing algorithm for wave propagation in anisotropic inhomogeneous materials are discussed Spies [19] studied elastic wave propagation in

homogeneous and layered transversely isotropic media using plane wave solutions and Gaussian wave packets Rudzki [20] proposed Fermat's principle for anisotropic media

1.3 PRESENT WORK

In the present investigation , time-of-flight (TOF) tomography has been used to reconstruct slowness in a glass-epoxy composite domain containing an insert of a spherical steel ball We have taken cross ply composite with insert at center, so symmetry in TOF data is expected, and we use this as an assumption to complete the data set ART, that is explained in chapter 3, has been employed for reconstruction which essentially computes the slowness distribution in the domain from a numerous projection TOF data from each different view Laser Based Ultrasonics(LBU) , as discussed above, is used to generate A-scan images for excitations along 0, 90, 45, and 135 degrees with respect to x-axis TOF information is then extracted from those images One of the objectives of this work is to observe the variation in the response at the receiver end when the concerned ray passes through or bypasses the insert region

The present study has been conducted on a domain (Material glass/epoxy) with dimensions 30mm×30mm containing an inclusion of a spherical steel ball of 4 76mm diameter as shown in fig 4 1(b) For reconstruction purpose, the domain is divided in to 30×30 grids and the slowness for each grid is evaluated in the reconstruction process This analysis is repeated for four directions (views), namely 0, 90, 45, and 135 degrees with respect to the positive x-axis as shown in the figs 4 1(c)-4 1(f) We have taken four A-scan images at 0 and 90 degrees with 3mm ray spacing, while nine A-scan images with 2 12 mm ray spacing are considered for 45 and 135 degrees Finally, for reconstruction purpose 30 rays have been considered for 0 and 90 degree view, while 60 rays are considered for 45 and 135 degrees For each view number of rays are chosen such that each boundary pixel acts as a source with opposite one as receiver Rays other than those from A-scan image are assumed on the basis of symmetry considerations and in-between rays are fixed by linear interpolation

Numerical Simulation of a similar object is performed to check the accuracy of the various algorithms and to compare with the experimental results

1.4 THESIS ORGANISATION

The various chapters in the thesis deal with the following aspects

- Chapter 2 presents the basics of laser ultrasonics
- Chapter 3 deals with the experimental set-up and procedure
- Chapter 4 deals with various ultrasonic tomographic reconstruction techniques
- Chapter 5 presents results and discussion of the present work
- Chapter 6 finally concludes the present work and gives suggestions for future work

Chapter 2
BASICS OF LASER ULTRASONICS

2.1 INTRODUCTION

Laser (Light Amplification by Stimulated Emission of Radiation) is a device that generates or amplifies light, just as transistors generate and amplify electronic signals at audio, radio or microwave frequencies Here, light must be understood broadly, since lasers have covered radiation at wavelengths ranging from infrared range to ultraviolet and even soft x-ray range The term ultrasonics is used to describe mechanical wave propagated in gases, liquids or solids at frequencies above the upper limit of human hearing i e 20KHz and up to 400MHz Because the characteristics of these waves are influenced by the mechanical properties of any medium through which they pass, one can use ultrasonics to investigate the properties of that medium

The laser-based ultrasonics (LBU) is the technique, in which laser beam interaction with the surface of the test sample is substituted for piezoelectric transducers for launching and probing elastic waves Since they do not require any mechanical contact, these techniques are very attractive For example, in the field of NDT, the association of laser generation with optical detection provides a completely remote ultrasonic system Other fields of applications are material evaluation, acoustic emission photo thermal microscopy and acoustic field imaging According to the intensity of the laser, the impact generation method may be classed in two main categories thermoelastic regime and ablation regime In the field of NDT, surface damage is avoided by means of specific techniques In concrete testing, the structure can tolerate some surface imperfection There are different methods applied, for example, one uses shock waves, which are generated by laser impact on the sample and optical detection (interferometrics or non-interferometrics), which monitors the induced surface Other methods are used incorporating contact ultrasonic probes working as receivers or transmitters Hence, this method needs no contact medium and the source can be some meters away, it is used

especially for applications such as NDT of systems at high temperature

2.2 MAIN PROPERTIES OF LASER LIGHT

Lasers are characterized by a number of key optical properties, most of which play an important role in the interaction with ultrasonic fields. Their four major optical properties are

1. Monochromaticity
2. Coherence
3. Directionality
4. High Intensity or Brightness

2.2.1 Monochromaticity

Monochromatic means the same frequency. Light from sources other than lasers covers a range of frequencies. True single-frequency operation of a gas laser can be achieved by careful design. Monochromaticity is reduced by multimode operation of a laser. A small He-Ne laser generally has three or four longitudinal modes excited with a spacing of a few hundred MHz, depending on the cavity length. This still gives a bandwidth of a few parts in 10^6. Solid-state lasers tend to have rather large frequency spreads

Monochromaticity is important for some ultrasonic applications, in particular the interferometric measurement of ultrasonic fields. Firstly, it is necessary in order to obtain high coherence, and secondly, it enables accurate absolute measurements of ultrasonic displacement to be made, since calibration is against the wavelength of the light. Monochromaticity is of less importance for the generation of ultrasound by laser

2.2.2 Coherence

Coherence means the same order or as a copy of the other photon and in phase with the other photon. Coherence is an important property when it comes to building an optical

system to detect ultrasonic waves In simple words, coherence is used to describe how well a wave disturbance at one point in space or time correlates with the disturbance at another point If there is a well defined phase relationship between the light at two different points in space (i e two light beams), or at two different times (i e one beam split into two with a delay between the parts, as is typical in an interferometer) then the two light disturbances can be brought together to produce a predictable interference pattern If the light is completely incoherent so that there is no predictable relationship (i e random phase) between the two disturbances, no interference fringes will be formed Fig 2 1 shows the comparison between the ordinary light and laser light

Coherence is important to the reception of ultrasonic waves by laser Most techniques involve some form of interferometer, in which good coherence between probe and reference beam is essential Coherence length is the distance of the origin of the beam to the farthest point at which the wave disturbance can be effectively correlated with the disturbance at its starting point Conventional monochromatic light cannot be used because their coherence length is only of the order of millimeters The use of a gas laser however enables use of a longer probe than reference beam This means that a compact instrument (incorporating all except the probe beam) can be built, and that the distance to the sample is not critical

2.2.3 Directionality

Directionality is a function of the spatial coherence of the beam of light Laser beam is highly directional which implies laser light is of very small divergence because of the parallelism of the beam The radiation produced by a laser is confined to a narrow cone of angles The beam of divergence for a typical gas laser is of the order of 1 milliradian, although some commercial He-Ne lasers are available with divergences of a few tenths of a milliradian Comparable beam divergences are now available from pulsed solid-state laser systems It is only possible to attain such low beam divergence from conventional light sources by severe collimation, which leads to extremely low intensities The

diameter of the beam is typically about 1mm for a gas laser such as helium-neon, and in the range 1-20 mm for a pulsed solid-state laser

The light from gas and solid state lasers thus forms a highly collimated beam which is extremely valuable for laser ultrasonics since it enables the beam to be focused to a very small spot This means not only high spatial resolution, but also, in the case of ultrasonic displacement measurement by interferometer, the ability to collect a larger fraction of the scattered light from a rough surface, thereby increasing sensitivity For laser generation it indicates that very high incident power densities are attainable Low beam divergence also means that the beam can travel distances of the order of several meters from the laser to the specimen without appreciable spreading and losses Thus both laser generation and reception of ultrasound can be made genuinely remote techniques.

2.2.4 High Intensity or Brightness

Intensity or brightness of a light source is defined as the power emitted per unit area per unit solid angle A laser beam is extremely intense, more intense than any other light source This is perhaps the property for which lasers are best known outside the field of optics Although the optical power output from a small helium-neon (He-Ne) laser may only be say 2mW, a beam diameter of 0 5mm leads to a power density of about 1 W cm^{-2} Such a beam can readily be focused by a simple lens to a spot of diameter 0 05 mm because it is monochromatic and coherent The incident power intensity is then 100 W cm^{-2} Focusing optics produces a beam of sufficient intensity to melt, cut or weld structural materials

Intensity is a most important property for laser reception of ultrasound, as sensitivity of a single mode laser interferometer system (defined as signal to noise ratio for a fixed bandwidth) increases with the square root of light intensity, provided other conditions remain constant The limiting factor becomes the intensity at which the specimen is damaged or otherwise adversely affected by intense irradiation Increase in power also brings penalties like increase in noise and multimode interference Intensity is also a

crucial factor in the generation of ultrasound by laser since incident power intensities typically in the range of 10^4-10^6 Wcm^{-2} are needed to act as a thermoelastic source of ultrasound The laser energy per pulse largely controls the ultrasonic amplitude in the thermoelastic regime The limiting factor is not the power that is available from commercial lasers, but rather the threshold for damage in the irradiated sample. Indeed, many pulsed lasers are too powerful for ultrasonic applications, and must be used at reduced power if the technique is not to be destructive

2.3 BASIC PRINCIPLE OF LASER OPERATION

The laser is a device, which amplifies the intensity of light by means of a quantum process known as stimulated emission A practical laser needs a means of amplification (i e stimulated emission) and a means for feeding the energy back into the system to build up sustained oscillation The operation of the simplest type of laser can be most readily understood in terms of a quantum mechanical model having say three energy levels E_0, E_1, E_2, such that $E_2 > E_1 > E_0$ (Fig 2 2) In reality, there may be more than three levels, but for present purposes, other levels are neglected The ground state E_0 is well populated, whereas the intermediate and upper states are more sparsely populated Suppose now the atom absorbs a quantum of incident radiation such that the atom is excited into the upper state From quantum theory, the radiation must have a frequency ν_p such that

$$h\nu_p = E_2 - E_0 \qquad (2\ 1)$$

Where h is the Planck's constant In laser terminology this process of absorption is known as 'pumping', so that ν_p is the 'pumping frequency' Pumping tends to equalize the population of two states so that E_2 becomes well populated This reverses the normal occupancy of E_2 and E_1 and is known as population inversion Emission (i e stimulated emission) can now occur in response to incident radiation, at a frequency ν given by

$$h\nu = E_2 - E_1 \qquad (2\ 2)$$

It can be noted that necessarily $\nu_p \geq \nu$, so that the pumping frequency must always be equal to or higher than that of the radiation to be amplified In order to obtain light of

sufficient intensity for practical use, there has to be some mechanism for feeding the energy back into the laser system and thereby building up the amplitude of oscillations in a resonant system. The usual way of obtaining sustained oscillations is to site a high performance mirror at each end of the lasing medium. In the simplest system, both mirrors are plane, and accurately aligned perpendicular to the axis of the laser. Thus, the light can be reflected backwards and forwards through the lasing medium. On each pass it stimulates further emission from the medium and is thus amplified in intensity.

2.4 LASERS FOR ULTRASOUND GENERATION

The simple laser arrangement will operate in a pulsed mode if it is pumped for example by a pulsed flash tube. Depending on the type of laser, pulses of duration typically 100 μs to 1ms can be obtained. Although high-energy pulses can be produced in this way, the normal mode is not particularly useful for laser ultrasonics because the pulse duration is too large. An additional technique, known as Q- switching or Q-spoiling, is needed to obtain pulses in the required 1-100ns range. The Q (quality) factor of a cavity resonator is the energy stored in the cavity divided by the energy lost from the cavity per round trip of the light within the cavity. Thus, if Q is low, the cavity oscillations are suppressed and the stored energy builds up within the lasing medium. When the Q is high, the cavity can support oscillations into which energy is supplied from the medium. Thus switching from low to high Q results in the rapid extraction of power from the laser cavity. Practical Q-switches are in the form of elements with variable absorption that are inserted between the mirrors. Two commonly used Q switches are the Pockels cell and bleachable (saturable) dye. Also of potential importance to non-contact ultrasonics are lasers that can be pulsed repeatedly. Adequate cooling in pulsed solid-state lasers is a problem. Hence gas lasers are preferred. However solid-state lasers can store higher individual pulse energies than gas medium lasers. Conventional ultrasonic inspection often uses repetition rates as high as 1-10 kHz for signal averaging purposes or for speed.

Laser generation of ultrasound does not impose very stringent conditions on the source laser. All that is required is the ability to deliver a reasonably high-pulsed energy density

to a small area of the specimen, where the pulse length is in the range of 1-100 ns As already mentioned, wavelength is not critical, nor is monochromaticity or coherence Most researchers have employed a solid state laser, either ruby or Nd YAG The Nd YAG laser has proved itself to be a versatile system under Q-switched conditions Adequate pulse energy can be obtained from Nd YAG lasers of modest size, while the pulse lengths are close to ideal for ultrasonic studies in metals However, the fundamental wavelength (1064nm) is in the near infrared, which makes alignment more difficult than with a visible laser, in addition to increasing the risk of accidental eye damage The Nd YAG laser is available with frequency doubling to give several harmonics of the fundamental frequency The frequency-doubled wavelength of 532 nm is in the middle of the visible spectrum, while the harmonics of 266nm and 355nm are in the ultraviolet zone

2.5 LASERS FOR INTERFEROMETRY

For applications like interferometry, where wavelength purity and coherence are important, continuous wave lasers are to be designed with special optical components The main problem is that a simple laser will excite a number of longitudinal and transverse modes The result is that energy is amplified over a narrow range of frequencies instead of the desired single frequency, giving rise to intermode beat frequencies, and there is a variable distribution of energy across the beam The generally preferred transverse mode (usually the lowest order mode with circular symmetry, TEM_{00}) can be selected, and higher order modes suppressed, by the use of at least one curved (concave) mirror at the end of the cavity and/or a suitable aperture within the cavity A multi-mode laser can be employed to minimize the multi-mode problem of longitudinal wavelengths in interferometry and then a balanced detection system and adjustment of the path difference between the two arms of the interferometer can be used to minimize the effects of intermode beats if necessary

The reception of ultrasound by laser is dependent upon all the fundamental properties of the laser monochromaticity, coherence, directionality and high power density Because

of its ready availability and excellent optical characteristics, notably monochromaticity and coherence, the He-Ne laser has dominated much of the work This system is however somewhat limited with regard to maximum power which controls sensitivity The other choice is the argon ion laser, which not only can deliver higher power, but also inherently more sensitive because of its shorter wavelength Argon ion lasers are however very bulky and noisy The CW Nd YAG laser is also available as a solid-state option, although it suffers from a number of drawbacks including bulk

2.6 LASER-IRRADIATED ULTRASOUND MODES

Laser ultrasonics are based on the phenomenon that laser irradiation onto a solid surface generates ultrasonic waves in the solid Fully non-contact generation and detection of ultrasonic waves can be realized by combining with optical (laser) interferometer for ultrasonic detection Thus, laser ultrasonic NDE could be applied to materials and structures in hostile environments, such as very high temperatures, or to components having complex geometries A laser emits a beam of coherent radiation, whose wavelength may be in the infrared, visible or ultraviolet part of the electromagnetic spectrum When this is incident on a solid sample, in general some of the energy is absorbed by various mechanisms, depending upon the nature of the sample and the frequency of the radiation, while the remainder is reflected or scattered from the surface Three basic mechanisms have been illustrated below

(I) The Thermoelastic Regime: At lower incident powers, electromagnetic radiation from the laser is absorbed in the surface region of a sample, causing localized heating as shown in Fig 2 3 Thermal energy then propagates into the specimen as thermal waves The heated region undergoes thermal expansion and thermoelastic stresses generate elastic waves (ultrasound), which propagate deep within the sample For typical Q-switched laser pulse durations, the thermal wave field only extends a few micrometers even in good conductors Contrast the incidence of low frequency modulated light where the thermal field extends millimeters or centimeters and is itself useful for materials characterization

(II) The Constrained Surface Source· Constrained surfaces include coating the surface with a thin solid layer of, for instance, paint or rust and roughness, covering the surface with a transparent solid such as glass, covering the surface with a transparent liquid, and finally constraining a thin layer of liquid between a transparent solid and the sample All these four techniques for modifying the surface of the sample introduce large stresses normal to the surface, as shown in Figs 2 4 (a-d), which are otherwise absent for the thermo elastic source at a free source The form of the ultrasonic source is thus substantially modified The different combination of stresses generates a different ultrasonic sound field, with considerable enhancement in compression-wave amplitude, especially propagating normal to the surface The constrained surface source generates a sound field more akin to that of ablation, but at lower power densities and without any damage However, the need to constrain with for instance a liquid, reduce the usefulness of the laser ultrasonic source for many non-destructive applications

(III) The Plasma Regime: At higher incident powers, surface melting and evaporation occurs, resulting in material ablation and the formation of plasma above the sample surface as shown in Fig 2 5 The momentum of the evaporated material exerts an opposite force on the sample, causing a reactive stress at the surface This generates an intense broadband ultrasonic source, whose strongest components are, directed normal to the surface The effects caused by the plasma generated in association with ablation in case of Q-switched lasers are

- The plasma exerts a high pressure on the surface, which in turn suppresses vaporization of the material by raising the boiling point of the material well above its normal value
- It absorbs light from the laser pulse, acting as a shield, but also becoming extremely hot
- As it expands it produces an impulse reaction on the surface
- It radiates some of its heat back on to the surface, maintaining its high temperature for some time after the incident laser pulse power has started to fall
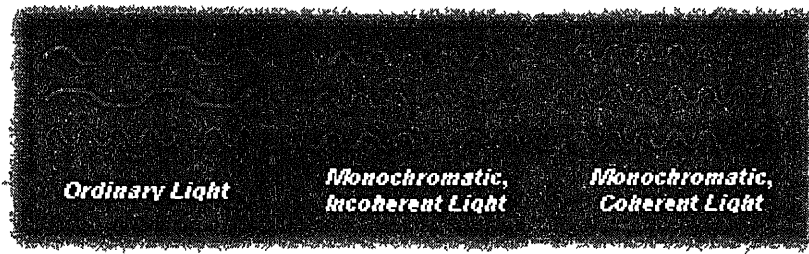
Fig 2 1 Comparison of ordinary light and laser light

Lasing
Transition
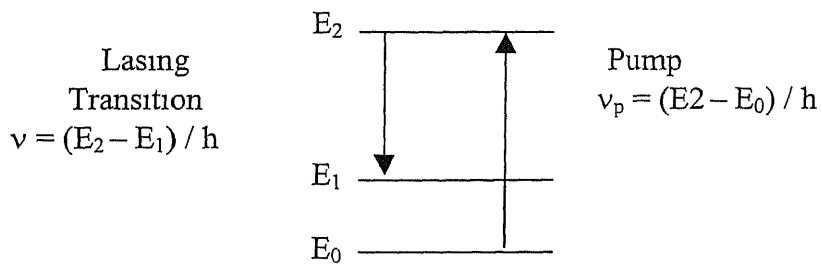$\nu = (E_2 - E_1) / h$

E_2

E_1

E_0

Pump
$\nu_p = (E2 - E_0) / h$

Fig 2 2 Simplified energy level diagram for a laser medium

Thermal Wave Field

Incident laser
Beam

Ultrasonic
Receiver

Absorption of Electromagnetic
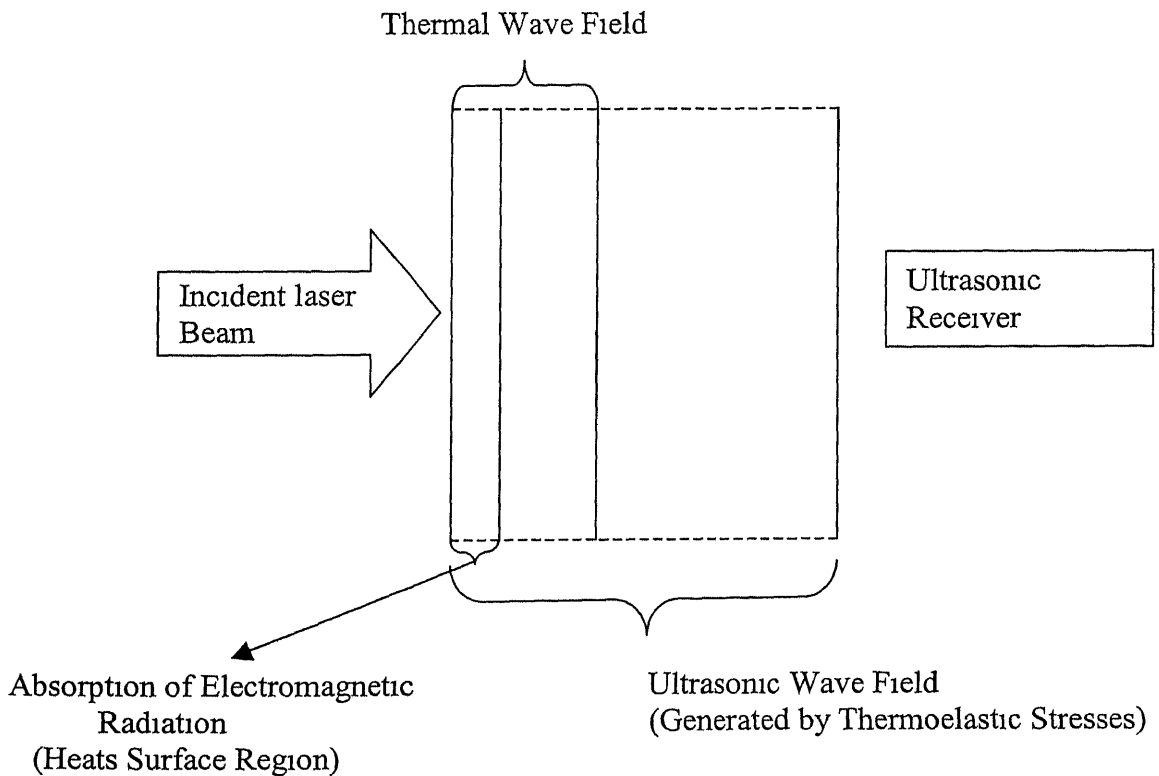Radiation
(Heats Surface Region)

Ultrasonic Wave Field
(Generated by Thermoelastic Stresses)

Fig 2 3 Thermoelastic regime

Incident
Laser Beam

Ablation of
Paint

Paint Layer

Thermoelastic
Stresses

Net Reactive Stress

(a) Paint Layer

Incident Laser
Beam

Transparent Solid
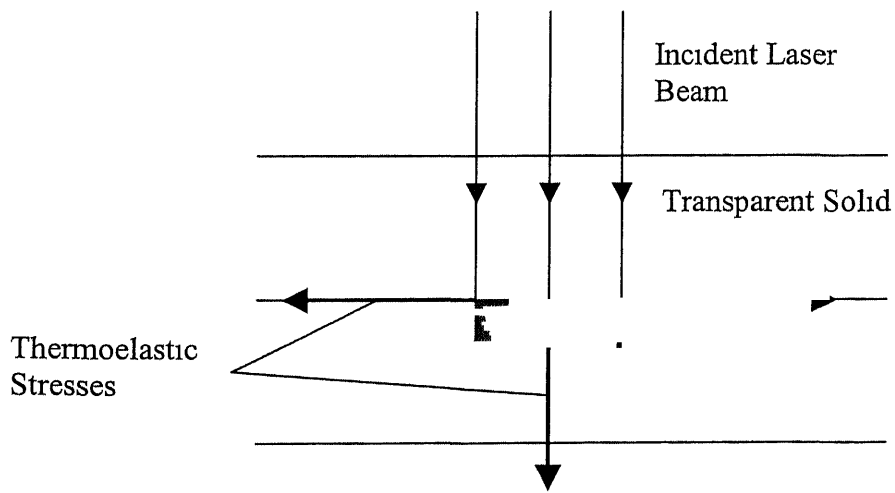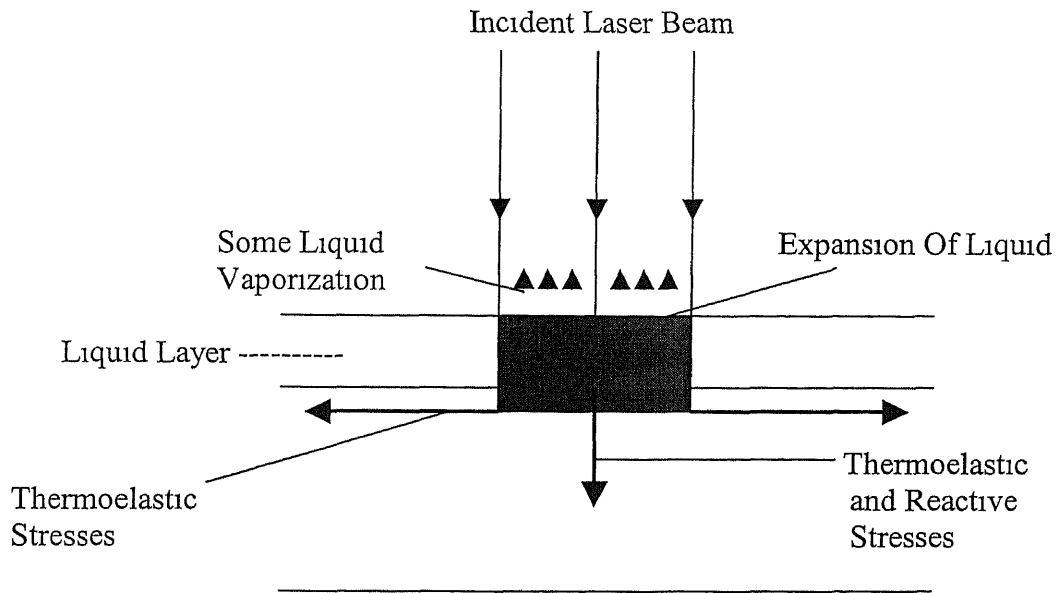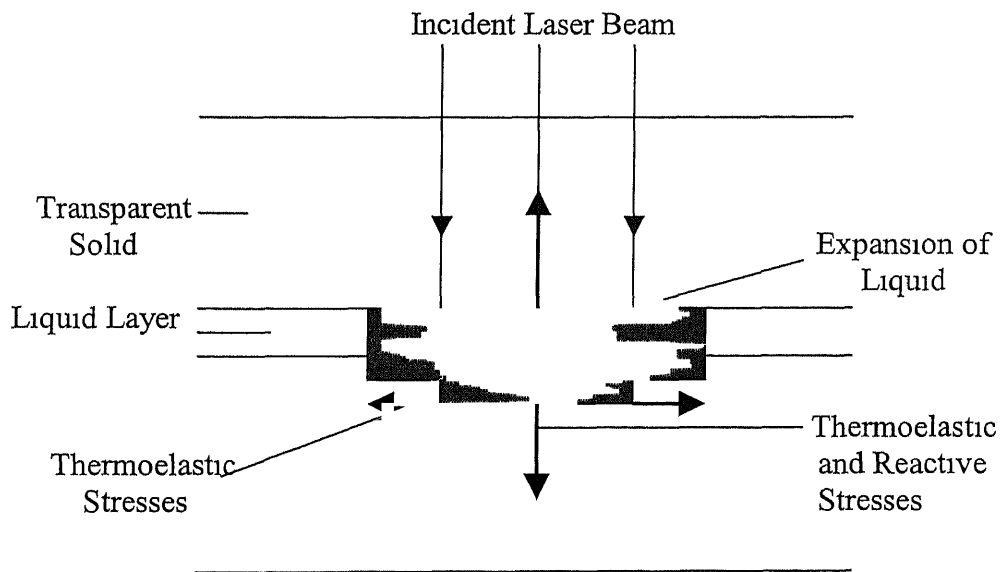
Thermoelastic
Stresses
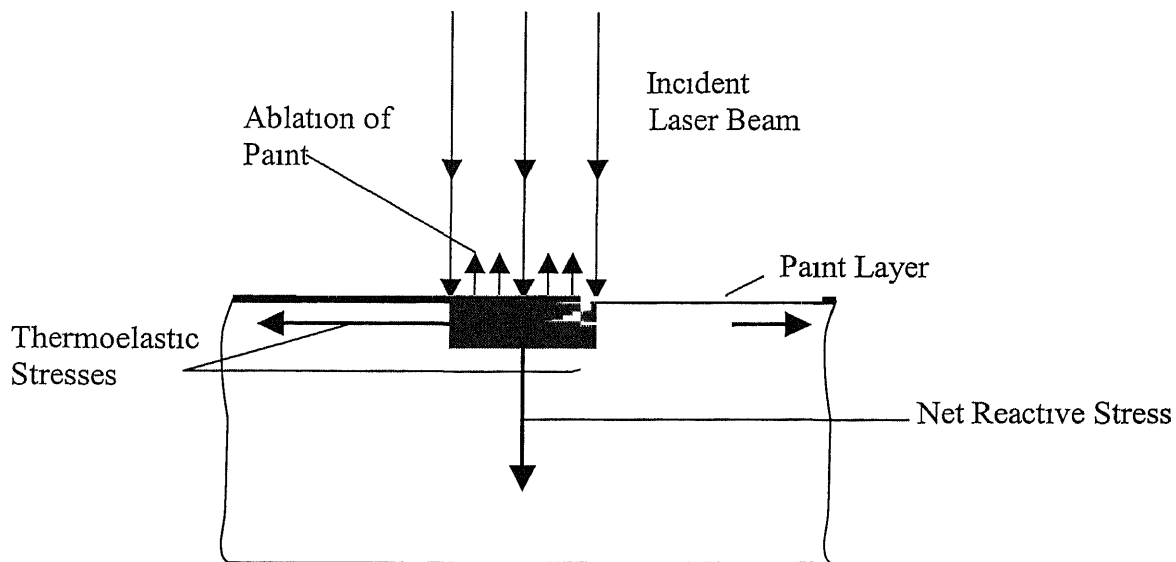
(b) Solid constraining layer

(c) Liquid Layer

(d) Constrained Liquid Layer

Fig 2.4 Schematic diagram showing stresses induced when a laser pulse is incident on a sample surface covered by (a) a thin layer of paint, (b) a thick transparent solid (c) a layer of liquid (d) a layer of liquid constrained by a transparent solid
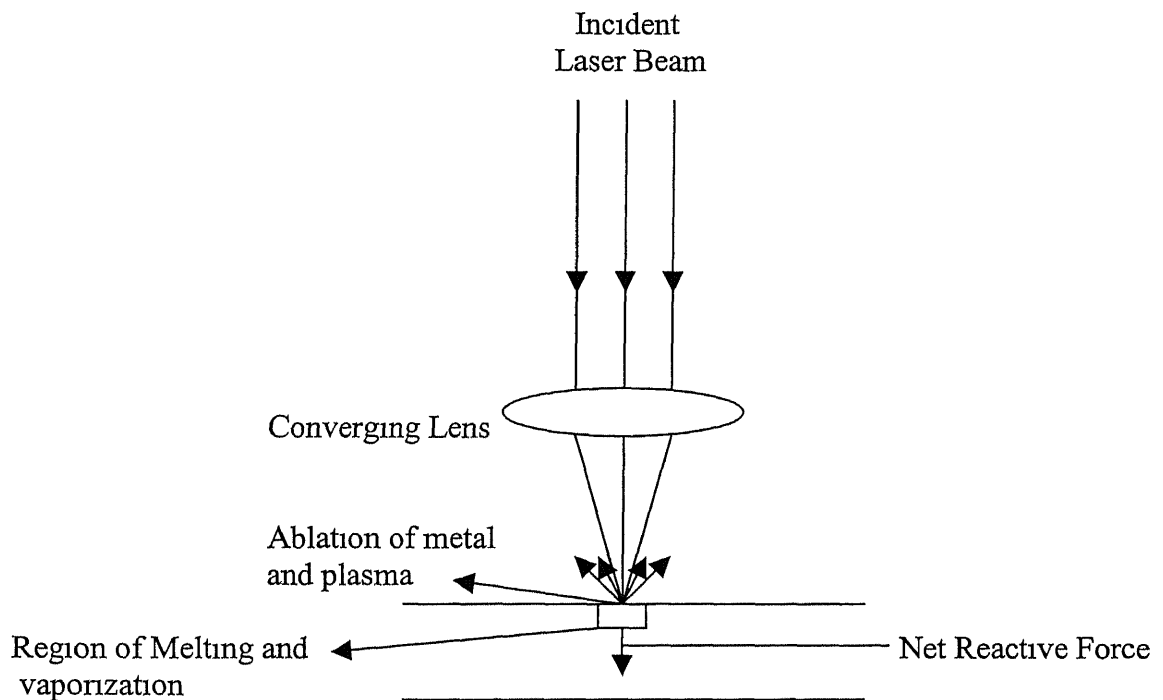
Fig 2 5 Schematic diagram to show ablation of surface material and net reactive force on sample

2.7 PRINCIPLE OF LASER INTERFEROMETRY

Optical interferometry is a very sensitive way of measuring displacement, but to be practicable for general use, it requires a highly monochromatic light source and thus the use of lasers is virtually essential Interferometers for the detection of ultrasonic movements of waves may be divided into two main types In the first type, light scattered or reflected from a surface is made to interfere with a reference beam, thus giving a measure of optical phase and hence instantaneous surface displacement The second type

of interferometer makes use of interference between a large number of reflected beams This is designed as a high-resolution optical spectrometer to detect changes in the frequency of the scattered or reflected light It thus gives an output dependent on the velocity of the surface The first type is the more widely used and the most practical at lower frequencies and with reflecting surfaces The second type offers a potentially higher sensitivity with rough surfaces, particularly at higher frequencies

For the detection of ultrasonic waves at a surface, the techniques are admittedly insensitive compared with piezoelectric devices They do, however, offer a number of advantages

(1) They are non-contacting and thus do not disturb the ultrasonic field The point of measurement may be quickly moved and there are no fundamental restrictions on surface temperature

(2) High spatial resolution may be obtained without reducing sensitivity The measurements may be localized over a few micrometers if necessary

(3) As the measurements may be directly related to the wavelength of the light, no other calibration is required

(4) They can have a flat broadband frequency response, something difficult to achieve with piezoelectric transducers, particularly at high frequencies

2.8 HE-NE LASER HETERODYNE INTERFEROMETER

2.8.1 Working of Optical Heterodyne Probe

The system consists of a compact optical head and an electronic signal-processing unit The optical layout is shown in Fig 3 2 The laser beam emitted by the laser source, horizontally polarized, is directed in the interferometer by two deflecting mirrors The laser beam is split into two parts by the beam-splitting cube The *reference* beam is reflected by the beam-splitting cube and goes through the Dove prism It is then transmitted by the polarizing beam-splitting cube and deflected by the mirror on the photodetector The *probe* beam is transmitted by the beam-splitting cube and is

horizontally polarized. Its optical frequency is shifted in the Bragg cell, and transmitted by the polarizing beam-splitting cube. A quarter wave plate transforms the horizontal polarization into circular polarization. The lens focuses the beam on the surface of the sample. The probe beam is then phase modulated upon reflection on the sample by the mechanical displacement. After the second pass in the quarter wave plate, the direction of polarization becomes vertical. The probe beam is reflected by the polarizing beam-splitter on the photodetector. Just after the polarizing beam-splitter, the polarization of the probe and reference beam are respectively vertical and horizontal. These two beams can therefore not interfere. The analyzer selects a common component at 45° of the two polarizations, thus allowing interference. The photodetector delivers a beat signal at the frequency of the Bragg cell phase modulated by the mechanical displacement of the object.

2.8.2   Principle of Detection

The complex amplitude of a laser beam of frequency f_L can be written as

$$L = e^{2i\Pi f_L t} \tag{2 3}$$

This is divided in the interferometer into a reference beam and a signal beam, whose complex amplitude is

$$R = r\, e^{2i\Pi f_L t} \tag{2 4}$$

The reference beam does not experience any perturbation, however the signal beam experiences a frequency shift f_B in the Bragg cell. Upon reflection on the object, its phase is modulated by the displacement of the sample

$$\varphi(t) = 4\pi\, d(t)/\lambda \tag{2 5}$$

where, λ is the wavelength of the laser beam and $d(t)$ the mechanical displacement of the object. The complex amplitude of the signal beam is therefore

$$S = s\, e^{2i\Pi f_L t + 2i\Pi f_B t + i\varphi(t)} \tag{2 6}$$

The interference of the two beams on the photodetector produces an electrical signal at frequency f_B, phase modulated by the displacement of the object

$$I(t) = I_0 + i(t) \tag{2 7}$$

$$I(t) = k\cos(2\pi f_B t + \varphi(t)) \tag{2 8}$$

The useful signal is contained in the signal delivered by the photodetector as a phase modulation of the carrier frequency The signal processor delivers an electric signal proportional to the displacement of the object Half of the current $i(t)$ is filtered at the frequency f_B, and phase shifted by 90° It is then mixed with the other half, non perturbed, and yields a current

$$j(t) \propto \cos(2\pi f_B t + \varphi(t)) \times \cos(2\pi f_B t + \pi/2) \tag{2 9}$$

$$j(t) \propto 1/2[\cos(4\pi f_B t + \varphi(t) + \pi/2) + \cos(\varphi(t) + \pi/2)] \tag{2 10}$$

The signal at the frequency $2f_B$ is filtered, to give

$$s(t) \propto \sin\varphi(t) \tag{2 11}$$

If the displacement is very small compared to the optical wavelength, this signal can be written as

$$s(t) = k\,4\pi\,d(t)/\lambda \tag{2 12}$$

The final electrical signal is therefore directly proportional to the displacement of the object

2.8.3 Sensitivity

Laser ultrasonics suffers from a lack of sensitivity relative to conventional ultrasonics as the photon structure imposes a fundamental limit on the change in light levels during generation / detection of lasers

Overall sensitivity to flaws is given by

$$\text{Sensitivity} = T \times f(\sigma, A) \times R \tag{2 13}$$

Where T, $f(\sigma, A)$, R are terms related to the transmitted sound, the focal or imaging properties of the system determined by the flaw scattering σ and the focal aperture A, and the receiver sensitivity The generated signal can be improved using tailored surface coatings or by increasing the power of the generating source However, this approach is limited by the onset of ablation in the target

2.9 CLOSURE

In this Chapter, the basic theory of generation of ultrasonic waves by lasers and their detection using laser-based interferometers has been presented Some of the important properties of lasers related to aspects of generation and detection of ultrasonic waves have been discussed Advantages of using laser-based detectors despite poor detectivity and sensitivity have also been explained

Chapter 3

EXPERIMENTAL SET-UP AND PROCEDURE

3.1 INTRODUCTION

This chapter briefly describes the details of laser-based ultrasonic (LBU) set-up, developed for non-destructive evaluation (NDE) of composite materials and data acquisition procedure

Nd YAG pulsed laser is used to generate ultrasonic waves in materials or objects to be inspected Heterodyne type laser interferometer is used to detect the transmitted wave through the material, the signals are then amplified and digitized using a Yokogawa DL1740 Digital Storage Oscilloscope (DSO) The oscilloscope is triggered using a synchronization signal from the pockels cell of the pulsed laser The recorded waveforms through DSO are transferred to a HP Pentium III computer over an USB/Ethernet interface for subsequent storage and analysis The schematic layout of experimental set-up is shown in Fig 3 1 and photograph of the same is shown in Fig 3 3, while Optical Layout of Heterodyne Interferometer is shown in Fig 3 2 The scanning is done manually using two single axis micrometer controlled XYZ translator mounted on the Optical Test Bench A brief description of the components of the present set-up is given in the following paragraphs

3.2 EXPERIMENTAL SET-UP: LASER-BASED ULTRASONICS

3.2.1 Nd: YAG Pulsed Laser Ultrasonic Generator

The 5000 DNS series pulsed Nd YAG laser is built on a modular concept The optical configuration allows variable setting of the optical parameters It consists of three major components, the laser-head, the power supply and the cooling unit The heart of the

system is the pumping structure, which houses the Nd YAG rod and the flash lamp The lasers are built on an electro-optically Q-switched oscillator This oscillator uses a pockels cell Q-switch to produce pulses of high intensity and short duration (i e in the order of 5-7 ns) Q- Switched lasers are often used as a non-contact ultrasound source in non-destructive testing (NDT) of materials Q-switched lasers typically have nanosecond
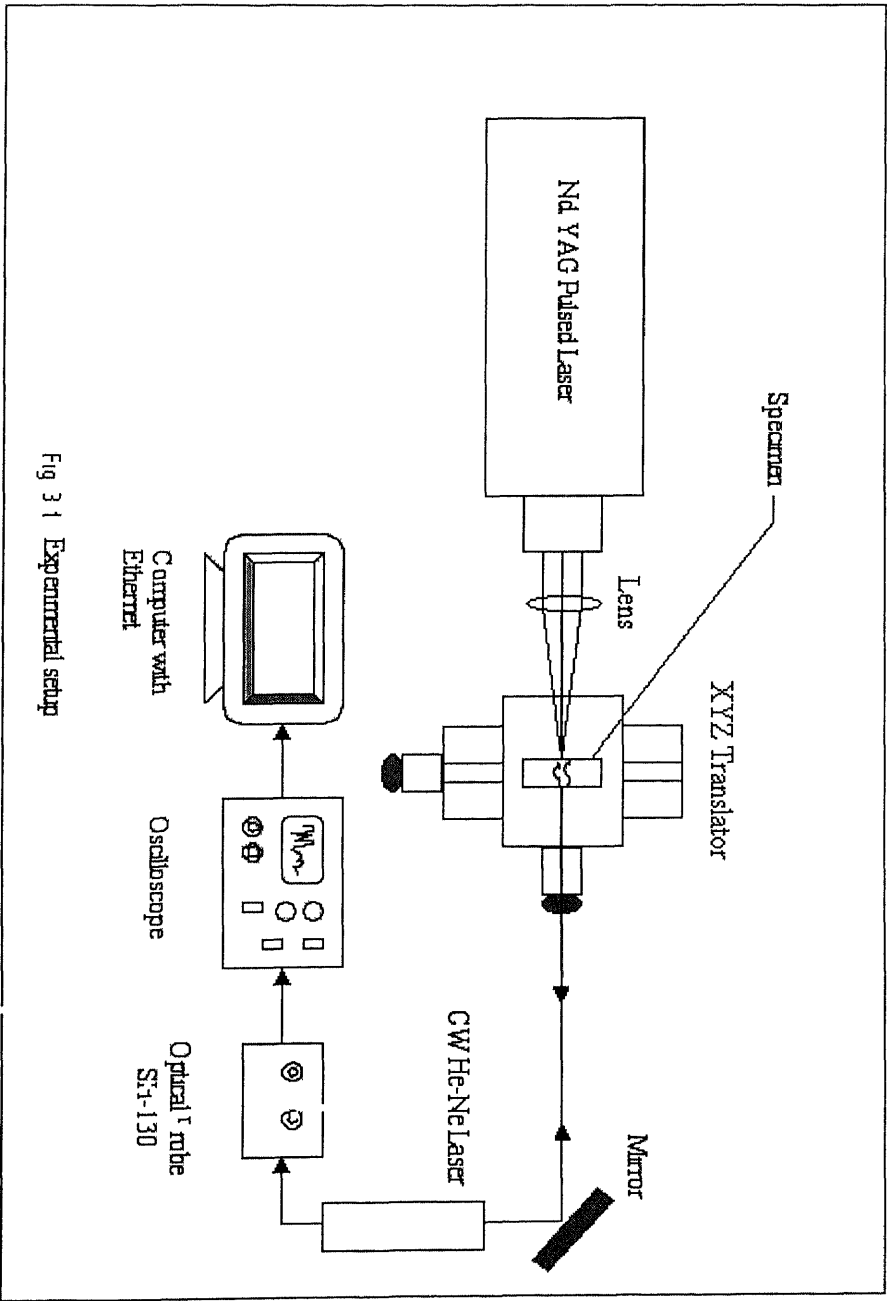

Fig 3 1 Experimental setup

(ns) pulse durations and generate broadband ultrasound waves, though longer laser pulses of 100 microseconds or greater have been used for NDE A variable reflectivity output coupler allows the extraction of high energy on a single spatial transverse mode This leads to laser beams of low divergence, and to high conversion efficiencies in the harmonic wavelengths (1064, 532, 355, 266 nm) Different harmonic generators extend the wavelength range to the second, third and fourth harmonics

The active medium of the laser operates on transitions of triply ionized Neodymium atoms (Nd3+), which take place of another ion (Yttrium) in the host Yttrium Aluminum Garnet known by the acronym YAG The laser operates as a 4-level system The intense broad-spectrum light of the flash lamp populates the upper level Once in the higher energy level, the Neodymium ions drop to a metastable level, producing a population inversion The lower level decays by a fast non-radiative process to the ground state The strongest Neodymium line is 1064 nm

3.2.2 Optical Heterodyne Laser (He-Ne) Probe

The SH-130 probe is designed to measure transient mechanical displacements of very low amplitude It is specially devoted to measure displacements generated by the propagation of an acoustic or ultrasonic wave The system consists of a compact optical head and an electronic signal-processing unit The optical head integrates high stability, low power laser source for fast detection with a high spatial resolution

The electronic signal processor delivers a response proportional to the displacement of the target, with a high bandwidth The output signal is automatically calibrated to give the absolute value of the measured displacement The principle of detection (heterodyne interferometry) makes the system insensitive to external vibrations The compactness of the system allows for a wide range of operating conditions

1- Single Frequency He-Ne Laser
2- Deflecting Mirrors
3- Beamsplitter
4 Dove Prism
5 Polarising Beamsplitter
6- Erase Coil
7 Quarter Wave Plate
8- Focussing Lens
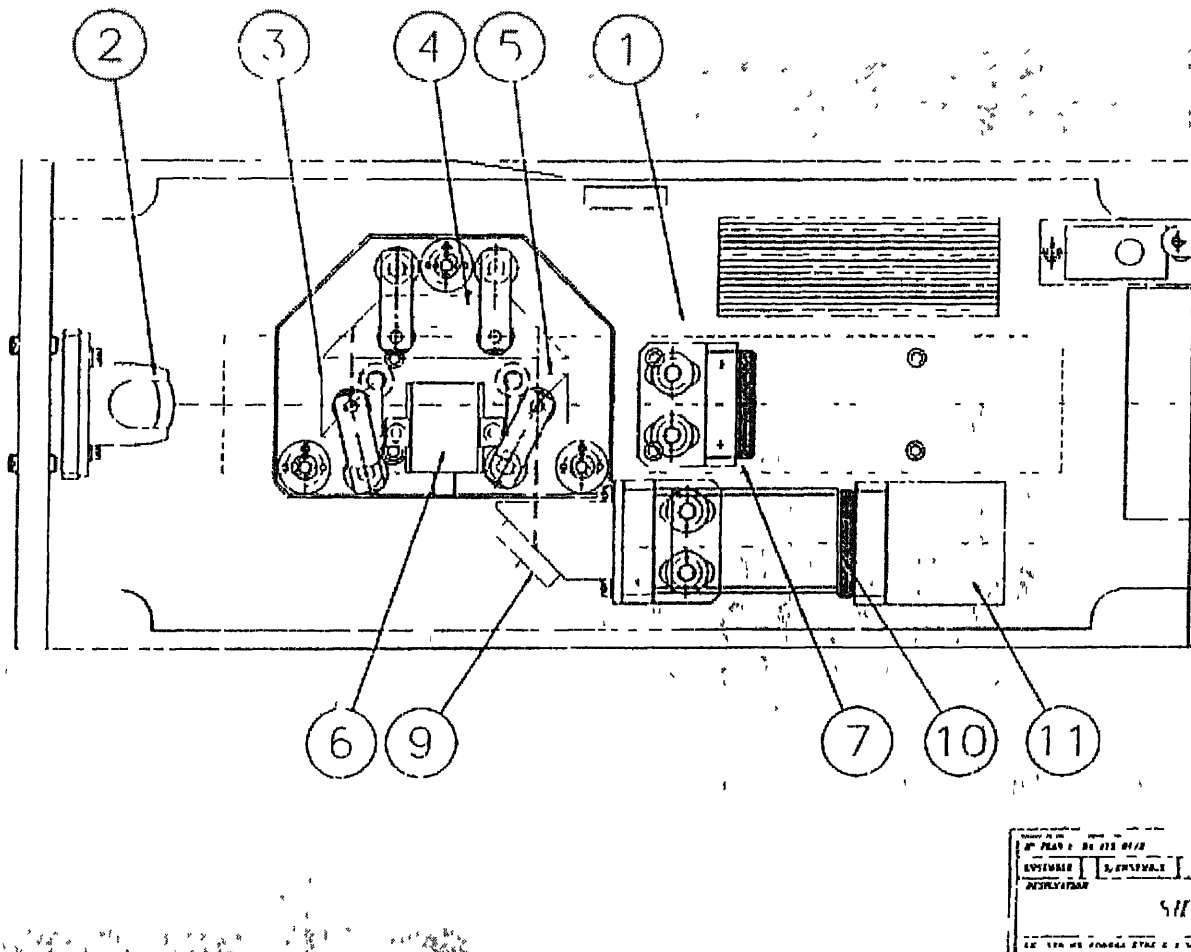9- Deflecting Mirror
10 Analyser
11- Photodetector

Figure 3 2 Optical Layout of Heterodyne Interferometer

3.2.3 Digital Storage Oscilloscope

The set-up utilizes a Yokogawa DL1740 (four channel, one GSa/sec, 500 MHz) Digital Storage Oscilloscope, having built in Zip drive, Ethernet, USB, GPIB and Serial Ports for communication with external PC's/ systems
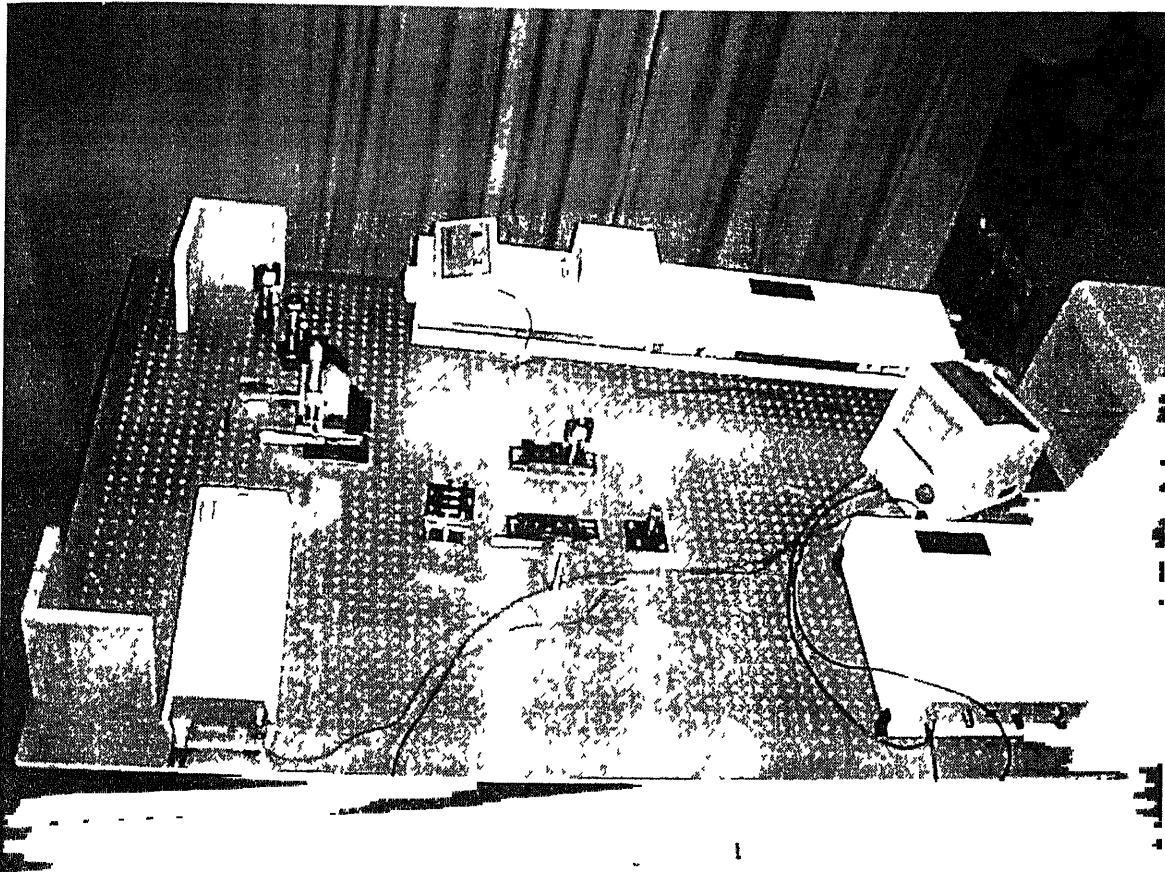
Figure 3 3 Photograph of experimental set-up

3 2 4 Computer

The DSO is interfaced to a Pentium III based PC and the data is transformed on-line using communication ports (Ethernet)

3.3 EXPERIMENTAL PROCEDURE (LBU)

3.3.1 Calibration of Set-up

The system was checked for calibration before scanning the specimen The procedural steps involved to check for calibration are as follows

(1) Alignment of the SH-130 Optical Probe This involved optimizing the control signal by adjusting the orientation of highly reflective mirror and fine-adjustment of its distance from the focusing lens (The focal length of the focusing lens is around 215 mm)

(2) The photo detector output was measured without going through the signal processor This was found to be 310 mV (as per specifications) The DSO image is shown in Appendix 'A'

(3) The output was then taken through the signal processor with the automatic gain control switched on The measured signal was found to be in excess of the stipulated signal level of 630 mV peak to peak on 50Ω (found to be 730 mV) This was adjusted using the adjustments available in the signal-processing unit The DSO image is shown in Appendix 'B'

3.3.2 Preparation of Specimens

The present ultrasonic non-destructive evaluation was done on composite specimens implanted with artificial inclusions like metal inserts The specimens were prepared by hand lay up technique, using woven glass fabric as the reinforcing material and epoxy resin as the matrix material Resin used being LY556, hardener HT976 and accelerator

XY73 all manufactured by Ciba Geigy (India) The curing was done at 120° C and 5 atm pressure for one hour followed by one hour at 150° C and 5 Atm pressure and left to cool to room temperature at same pressure overnight

The dimensions of the finished specimens were 30 x 30mm^2 Model specimens were prepared with a central mild steel insert to simulate presence of flaws or defects The metal inserts, spherical in shape, about 4 76mm in thickness was introduced centrally in the thickness direction (in between plies 36 and 37) All the specimens were cast with 72 plies with a final thickness of around 20 mm

3.3.3 Scanning Procedure

The specimen to be investigated was cleaned and the area under investigation was marked To get good signals, the portion of the specimen facing to the Ne-He laser was pasted with retro-reflective tape The He-Ne laser was switched on to align the CW laser beam with the marked point of investigation to obtain good information regarding the wave propagation Then the Nd YAG laser was focused onto the specimen using an arrangement of optical mirrors and lenses (as shown in figure 3 1) so that it acts as a point source and is perpendicular to the irradiated face of the specimen The alignment of Nd YAG and He-Ne laser was ensured by focusing the Nd YAG laser on the marked point of investigation on the opposite face of the specimen The power level of the laser was adjusted to ensure thermoelastic region so that there was no ablation of the specimen The scanning was performed at setting corresponding to 1064nm wavelength for the Nd YAG laser The He-Ne laser was focused on the opposite side of the specimen at the focal length of the collection lens (approx 215mm) The output of the Optical probe was fed to the electronic signal-processing unit The electronic signal processor delivers a response proportional to the displacement of the target, with a high bandwidth The output signal was automatically calibrated to give the absolute value of the measured displacement This was fed to the Digital Storage oscilloscope (DSO) where it was displayed and storage of the data was carried out on-line in the PC interfaced to the DSO

3.4 CLOSURE

In this Chapter, the details of experimental set-up and scanning procedure are presented for the Laser-Based Ultrasonic (LBU) set-up Experimental procedure for data acquisition is also explained

Chapter 4

ULTRASONIC TOMOGRAPHIC
RECONSTRUCTION

4.1 INTRODUCTION

The technique of Computerized Tomography (CT) has established itself as a leading tool in diagnostic radiology over the past twenty years and it is gaining importance in the nondestructive evaluation area in a variety of situations In conventional projection radiography, the result is just obtained just in the form of a shadowgraph requiring a lot of interpretation CT, however, uses tomographic reconstruction to combine the information from multiple projections Thus, the CT information is displayed quantitatively as a reconstructed slice plane of the object and it can provide accurate quantity measures of material characteristics in small volume elements of the component CT was originally conceived for X-rays, but in recent times, CT has been implemented for other energy sources such as acoustic, laser, microwaves etc Among these, acoustic tomography (especially using ultrasonic waves (UCT)) has special importance in application to NDE Like X-ray CT, the physics of ultrasonic CT involves two steps

1   The measurement of the time of flight data for the wave passing trough a number of different paths through a test object, followed by
2   The reconstruction of slowness coefficient values at all the interior points from the data collected in step (1)

Thus, acoustic tomography can be defined as a technique to determine values of a spatially varying acoustic parameter of interest across a slice through an object Waves travel through the sample (from a series of source locations) to receivers at appropriate positions around the object The source and the receiver locations are chosen such that the rays pass through a large portion of the object volume as possible The relative

positioning of the source and receiver should also conform to any requirement for regular positioning in the reconstruction procedure As the source and the detector are moved around the object, a number of individual projections (or measured data sets) are obtained Each projection is composed of a transmitted intensity pattern, which depends on the path concerned After completing a scan consisting of a number of projections, the distribution of the slowness coefficients within the object is reconstructed by one of the several reconstruction techniques

The major problem in applying UCT is that ultrasound does not travel strictly in linear fashion and suffers scattering, ray bending and the diffraction at the interface of any dissimilar material In medical applications, however, UCT can be used safely in soft tissues imaging where deviation from linearity in propagation is minimal Among industrial applications, practical material characterization problem such as study of residual stress distribution has also been tackled by UCT With proper guideline for collecting projection data and proper modification in the reconstruction technique, accurate quantitative evaluation of the material properties of the object slice can be accomplished

4.2 RECONSTRUCTION METHODS

Tomography can be classified into (a) transform (b) series expansion and (c) optimization methods Transform methods in general, require a large number of projections for a meaningful answer However, in most of the cases it is not practicable to record such a large number of projections partly owing to inconvenience and partly due to time and cost Hence, as a rule requirement of a large number of projections is not desirable and one must look for methods that converge within a few iterations Limited-view tomography is best accomplished using the series expansion method As limited data tomography does not have a unique solution, the algorithms are expected to be sensitive to the initial guess of the field that starts the iterations Optimization-based algorithms are known to be independent of initial guess, but the choice of optimization function plays an important role in the result obtained Depending on the mathematical definition used, the

entropy extremization route may yield good results, while the entropy minimization principle may be suitable in other applications For the algebraic technique considered in the present study, an unbiased initial guess such as a constant profile was seen to be good enough to predict the correct field variable Tomography, being an inverse technique was seen to preserve the noise in the initial data However, the dominant trend in the field variable was captured during tomographic inversion Actually the problem of reconstruction is a problem of inversion of the rectangular matrix Iterative techniques that are used in tomography can be viewed as developing a generalized inverse of the matrix The general purpose matrix libraries cannot be used to invert them since they are highly ill conditioned and rectangular in structure The tomographic algorithms can be seen as a systematic route towards a meaningful inversion of the matrix

4.2.1 Algebraic Reconstruction Technique (ART)

ART is one of the most popular techniques based upon a row action method for solving large, sparse systems It assumes a solution for the image matrix and iteratively compares projections through the image to the measured projection data With each iteration the image matrix is altered until a match between the calculated and measures projections are within acceptable accuracy This technique is useful when limited angles of projections are available and can become highly computation intensive

In tomography, projection data (p) represents an integrated information resulting from interaction of source radiation with the material, and is expressed as

$$p = \int_s f(x, y) ds \qquad (4\ 1)$$
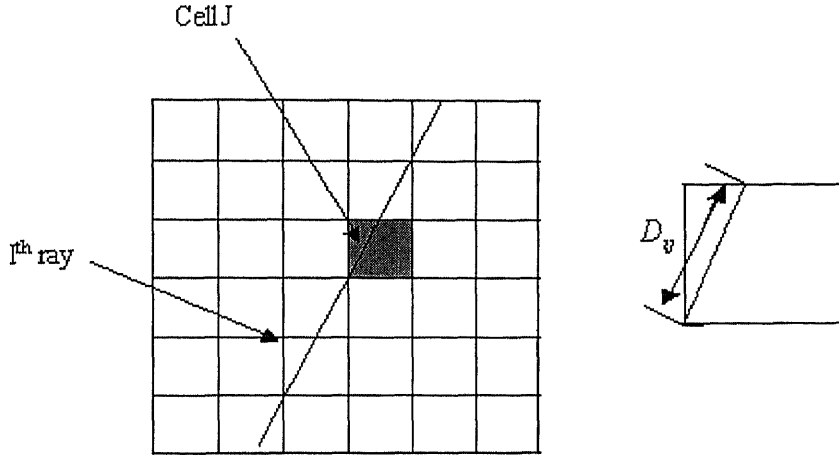
Figure 4 1 Weight function D_{ij} for i^{th} ray and j^{th} pixel

The iterative reconstruction methods of tomography are based on the descretization of the cross sectional plane by a square grid as shown in the Fig 4 1 The length of the intercept of an ith ray with the jth pixel in a given projection is called the weight function $\left(D_{ij}\right)$ If f_j is the field value in the jth pixel, the ith projection is given as

$$p_i = \sum_{j=1}^{N} D_{ij} f_j, \quad i=1,2, \quad ,M \qquad (4\,2)$$

where M is the total number of rays and N is the number of pixels

It is required to collect the projection data over a number of view angles to carry out tomographic reconstruction When ultrasound wave is used as a source of radiation, f(x, y) and p_i are usually taken to be the slowness field (inverse of group velocity) in the object and time-of-flight (TOF) respectively The aim in tomography is to obtain f(x, y) from given p_i The conventional algebraic reconstruction technique (ART) involves four major steps

1   Initial assumption of the object field,

2   Calculation of correction,

3   Application of the correction and

4 Test for convergence

Typically, in Gordon ART, the field values f_i in pixels are updated for k^{th} iteration using correction term as

$$f_i^k = f_i^{k-1} + \frac{p_i - \langle D^i, f^{k-1} \rangle}{\|D^i\|^2} D_{ij} \tag{4 3}$$

Here the inner product notation is used in the following sense

$$\langle D^i, f^{k-1} \rangle = \sum_{j=1}^{N} D_{ij} f_j^{k-1} \tag{4 4}$$

Where

$$D^i = \sum_{j=1}^{N} D_{ij} \tag{4 5}$$

and

$$\|D^i\|^2 = \langle D^i, D^i \rangle \tag{4 6}$$

To tackle the problem for inconsistent system of equations, a modification in the ART discussed above, is necessary The behaviour of ART algorithm for inconsistent systems when relaxation parameters are allowed was discussed by Eggermont et al [1981] Relaxation parameters area sequence of real numbers usually confined in some interval The modified step (with relaxation parameter) for updating the iterate can be expressed

$$f^k = f^{k-1} + \lambda_k \frac{p_i - \langle D^i, f^{k-1} \rangle}{\|D^i\|^2} D_{ij} \tag{4 7}$$

where

$$\varepsilon_1 \leq \lambda_k \leq 2 - \varepsilon_2 \qquad\qquad \varepsilon_1, \varepsilon_2 > 0$$

Following are some of the other ART algorithms

- Simple ART

It is similar to Gordon ART, except the modification step (with relaxation parameter) is given as

$$f^k = f^{k-1} + \lambda_k \frac{p_i - \left\langle D^i, f^{k-1} \right\rangle}{D^i} D_{ij}$$ (4 8)

- Gilbert ART

Gilbert (1972) has developed independently a form of ART called the simultaneously iterative reconstruction technique (SIRT) In SIRT, the elements of the field function are modified after all the correction values corresponding to individual rays have been calculated The algorithm is similar to ART but the correction is applied as given below

* Identify all the rays (N_C^j) passing through a given cell and the corresponding

D^i and $p_i - \left\langle D^i, f^{k-1} \right\rangle$

* For each cell j apply the algebraic sum of all possible correction terms as

$$f^k = f^{k-1} + \sum_{ic=1}^{N_c^j} \lambda_k \frac{p_i - \left\langle D^i, f^{k-1} \right\rangle}{\left\| D^i \right\|^2} D_{ij}$$ (4 9)

4.2.2 MART ALGORITHMS

The difference between ART and MART algorithms lies in the manner in which the corrections are applied to guessed field values The corrections are additive in former, while multiplicative in the latter These algorithms are essentially iterative in nature, but intermediate steps may also involve repetitive calculations To identify the iterative loop,

start_ and close labels with statement numbers have been indicated in the description of each algorithm

The MART algorithms are first summarized Let ϕ_{i_θ} be the projection due to i^{th} ray in θ direction of projection and $\tilde{f}_i$ be the initial guess of the field value The projection $\tilde{\phi}_{i_\theta}$ using the current field value can be obtained numerically as

$$\tilde{\phi}_{i_\theta} = \sum_{j=1}^{N} D_{i_\theta,j} f_j \qquad\qquad i_\theta = 1,2, \quad ,M_\theta \qquad\qquad (4\ 10)$$

where M_θ represents number of rays along the θ direction The parameter to be varied in each loop is indicated in brackets

Start 1 Start iterations (k)

    Start 2 For each projection angle (θ)

        Start 3 For each ray (i_θ)

        Compute the numerical projection [Eq 4 4]

        Calculate the correction as

$$\Delta\phi_{i_\theta} = \phi_{i_\theta} \big/ \tilde{\phi}_{i_\theta} \qquad\qquad (4\ 11)$$

        Start 4 For each cell (j)

        If $w_{i\theta\ j}$ is nonzero then

MART1

$$f_j^{new} = f_j^{old} \times (\ 1\ 0 - \mu \times (\ 1 - \Delta\phi_{i_\theta}\ )) \qquad\qquad (4\ 12)$$

MART2

$$f_j^{new} = f_j^{old} \times [\ \ 1\ 0 - \mu \times \{\ D_{i_\theta,j}\ /\big(D_{i_\theta,j}\big)_{max}\ \} - (\ 1 - \Delta\phi_{i_\theta}\ )] \qquad\qquad (4\ 13)$$

MART3

$$f_j^{new} = f_j^{old} \times \big(\Delta\phi_{i_\theta}\big)^{\left(\mu D_{i_\theta\ j}/\big(D_{i_\theta\ j}\big)_{max}\right)} \qquad\qquad (4\ 14)$$

    where μ is relaxation factor

        close 4

close 3

    close 2

Check for convergence as

If

$$\text{abs}[(f^{k+1} - f^k)/(f^{k+1})] \times 100 \le e \tag{4 15}$$

where e is a suitable stopping criterion STOP

Else Continue

Close 1

Steps 3 and 4 form the essence of the reconstruction algorithm All three versions include the relaxation factor μ Typical values for relaxation factor reported are in the range 0 01-0 1, larger values leading to divergence It is to be noted that correction calculated in step 3 is the ratio of the recorded projection data $\left(\phi_{i_\theta}\right)$ and that calculated from guessed field namely, $\widetilde{\phi}_{i_\theta}$, which is being iterated The three versions of MART are In MART1, the weight function is prescribed in binary form, being unity if a pixel ray passes through a pixel and zero otherwise In MART2 and MART3, the weight function is calculated precisely as the ratio of the length of the ray intercepted by the pixel and the maximum dimension of pixel enclosed in it

4.3 Reconstruction errors

During the present work, the performance of reconstruction technique is evaluated both quantitatively and qualitatively The average EL1 and RMS EL2 error are used to measure performance and defined as

$$EL1 = \frac{100}{N(f_{\max} - f_{\min})} \sum_{i=1}^{N} \left(\left| f_{original} - f_{reconstructed} \right| \right) \tag{4 16}$$

$$EL2 = \frac{\sqrt{\dfrac{\sum_{i=1}^{N}(f_{actual} - f_{reconstructed})^2}{N}}}{f_{\max} - f_{\min}} \times 100 \tag{4 17}$$

4.4 CLOSURE

In this chapter various tomographic algorithms were discussed Error estimation of the independent parameters to evaluate the performance of the algorithm was included

Chapter 5
RESULT AND DISCUSSION

5.1 INTRODUCTION

Firstly, analysis of the signals (A-scan) obtained from Laser Based Ultrasonics (LBU) set-up is done to extract the Time of Flight (TOF) information for subsequent reconstructions Then, the reconstruction of slowness field of the crossection under consideration is performed using both ART and MART for different values of relaxation parameters and initial field values

As mentioned earlier, a Cartesian grid of square picture elements, called pixels, is introduced into the domain (30mm×30mm) of interest Number of rows and columns in the grid are 30 Thus the domain is essentially discretized into 900 pixels The numbering arrangements of the pixels, columns and rows have been chosen in the manner as shown in fig 5 1(a) The base material of the domain is glass/epoxy and it contains a cross section of steel ball as shown in fig 5 1(b)

The reconstruction is conducted from projection data Projections have been taken in four directions or views Four directions, namely 0 ^{0}, 90^0, 45^0, and 135^0 with the x-axis, of the views or rays have been used in this work

Finally, for reconstruction purpose 30 rays have been considered for 0 and 90 degree view, while 60 rays are considered for 45 and 135 degrees For each view number of rays are chosen such that each boundary pixel acts as a source with opposite one as receiver Source is considered to be the center of the boundary side of the pixel, so ray spacing for 0 and 90 degree is 1mm, while for 45 and 135 degree it amounts to 0 71mm Rays other than those from A-scan images are assumed on the basis of symmetry considerations and in-between rays are fixed by linear interpolation

5.2 EXPERIMENTAL RESULTS

5.2.1 RESULTS FOR EXCITATION ALONG 0^0

In this view four A-scan images are obtained from experiment performed on LBU set-up A-scan plots at the receivers for two representative cases are shown in fig 5 2 Case 1 and case 2 as shown in fig 5 2, are the A-scan plots at the respective receivers corresponding to the pulsed excitations at the extreme left pixel in the 5th and 14th row

For case 1 the ray (ideal travel path being assumed as linear and coinciding with the direction of excitation) has no intercept on the insert region as shown in fig 5 1(c), so the TOF obtained from the plot can taken as the time to travel 30mm of glass/epoxy The A-scan plot (case 1) shows one sharp signal which initiates at a time of 7 0 μs indicating the wave's arrival

Thus, the TOF, in this case is taken as 7 0 μs Case 2 corresponds to the ray traveling along the 14th row of the grid, which has an intercept on the insert zone In contrast to case 1, this plot shows signal initiating little later than 7 0 μs, at 7 2 μs, indicating the wave's arrival Thus, the TOF, in this case is taken as 7 2 μs

Rest of the two A-scan images for excitation along row 8th and 11th are similar to case 1 and TOF is taken as 7.0 μs Hence, it can be inferred that defect is present between 11th and 17th row

5.2.2 RESULTS FOR EXCITATION ALONG 90^0

In this view four A-scan images are obtained from experiment performed on LBU set-up A-scan plots at the receivers for two representative cases are shown in fig 5 3 Case 1 and case 2 as shown in fig 5 3, show the A-scan plots at the respective receiver ends

corresponding to the pulsed excitations at the extreme left pixel in the 5th and 14th column

For case 1 the ray (ideal travel path being assumed as linear and coinciding with the direction of excitation) has no intercept on the insert region as shown in fig 5 1(d), so the TOF obtained from the plot can taken as the time to travel 30mm of glass/epoxy The A-scan plot (case 1) shows one sharp peak which initiates at a time of 7 0 μs indicating the wave's arrival

Thus, the TOF, in this case is taken as 7 0 μs Case 2 corresponds to the ray traveling along the 14th column of the grid, which has an intercept on the insert zone In contrast to case 1, this plot shows signal initiating little later than 7 0 μs, at 7 2 μs, indicating the wave's arrival Thus, the TOF, in this case is taken as 7 2 μs

Rest of the two A-scan images for excitation along column 8th and 11th are similar to case 1 and TOF is taken as 7 0 μs Hence, it can be inferred that insert is present between 11th and 17th column Same TOF for both 0^0 and 90^0 views signify good experimental results as the composite is cross ply and hence nearly same results were expected

5.2.3 RESULTS FOR EXCITATION ALONG 45^0

In this view nine A-scan images are obtained from experiment performed on LBU set-up A-scan plots at the receivers for the nine representative cases are shown in fig 5 4 It can be inferred from 0 and 90 degree excitations that the insert is within a 6mmX6mm central region of the domain under consideration, so it is expected that only in the last two cases, viz 8th and 9th case, the ray has an intercept with the insert

Case 1 to case 7 denotes the signal at receiver end corresponding to pulsed excitation from 26th to 8th column on X-axis at a regular spacing of 3 columns between each excitation The TOF for each ray is the time of initiation of the signal, signifying the

arrival of ray   Case 8th and 9th correspond to the rays originating at 2nd and 5th column on the X-axis

5.2.4 RESULTS FOR EXCITATION ALONG 135^0

TOF data for 135^0 are assumed on the basis of experimental results along 45^0 The data set is taken same as for 45^0

5.3 RECONSTRUCTION RESULTS

Reconstruction of slowness field from the TOF data set can be performed by using different variations of ART and MART Simple ART is used for reconstruction purpose The total number of rays used for reconstruction, as discussed above amounts to 180, 30 each for 0 and 90 degrees, while 60 each for 45 and 135 degrees In the following sections, the effect of change of relaxation parameter, initial guess and algorithm on the reconstruction is noted

The drawback of using isotropic algorithm to study anisotropic material like composite, is to compromise on the actual field values of the material crossection and to some extent have to worry about the presence of unexpected defects, but the ease of working with simple assumptions such as straight ray approximation, and the successful determination of defect location and geometry, along with the anisotropy present makes the study worth pursuing Although, some more analysis is required with the assumptions, but simple assumption with detailed analysis can be woven into a successful, and more important a general tool

5.3.1 RECONSTRUCTION USING ART WITH DIFFERENT RELAXATION PARAMETERS

Reconstruction results for different relaxation parameters are shown in figs 5 5(a)-5 5(h) For these reconstructions initial guess (f') is a square matrix with 0 21 as the value of each element and stopping criteria is given as,

$$\text{abs}[(f^{k+1} - f^{k})/(f^{k+1})] \times 100 \leq e \tag{5 1}$$

where f^{k+1} and f^{k} are the field values after k+1 and kth iteration respectively, e is a suitable stopping criteria, here it's value is 0 1

Fig 5 5(a) - 5 5(h) are the reconstructions for relaxation parameters ranging from 1 99 to 0 0001 As can be seen from the reconstructions, the results significantly improve on decreasing the value of relaxation parameter and confidence for the presence of central circular defect increases on going for values lower than 0 5 Fig 5 5(f) is the reconstruction for λ=0 01, field values in the central region are in striking contrast with rest depicting presence of an extended central defect Figs 5 5(g) and 5 5(h) are for λ=0 001 and λ=0 0001, a near circular defect of size from 4 to 5mm can be inferred from them

Longitudinal wave velocity in glass epoxy is around 4200m/s and longitudinal wave velocity of steel is around 5000m/s (For subsequent analysis these values are taken as reference) Figure 5 6(c), depicts some regions where longitudinal wave velocity in glass epoxy is exactly matching with nearly 18% error in reconstruction for steel

ART have many variations such as Gordon ART, Gilbert ART etc, difference between them lies in the correction value and/or implementation stage Until now, simple ART was used for reconstruction, now implementation of Gordon ART and Gilbert ART will help in comparing the results Fig 5 6(a)-5 6(d) shows the reconstruction using Gordon ART Figure 5 6(d), shows some regions where error in Longitudinal wave velocity in glass epoxy is below 10% and nearly 9% error in reconstruction for steel Fig 5 7(a)-5 7(d) shows the reconstruction using Gilbert ART On considering Fig 5 7(d) it can be

seen that the error in longitudinal wave velocity in glass epoxy region is higher than for Gordon ART, while there is a slight reduction in error for insert region reconstruction values The corresponding reconstructions using Simple ART figs 5 5(a)-5 5(h), shows results nearer to Gilbert ART

It can be seen that the relative values of longitudinal velocities in the defect and base material are on the wrong side, but because of the nature of defect and the data acquisition and reconstruction method, defect is considered, as including, also the region considerably influenced region with the implantation of insert

So, it can be said that the TOF data is an information about the influence of affected region on the incident ray In that sense some meaningful results can be generated without loss of generality Here broken fibres, resin rich zone and bypassing of the ray can be attributed to greater slowness values of the defect

5.3.2 RECONSTRUCTION USING MART WITH DIFFERENT RELAXATION PARAMETERS

Results are here augmented using MART algorithms and observe differences, if any, in reconstruction Figures 5 8(a)-(h) are the reconstructions using MART1 for λ's, varying from 1 99 to 0 0001 As can be seen from the figs the reconstruction (On considering only the defect geometry, condoning the slowness values) didn't deteriorate for higher values of λ as observed using ART and good defect reconstruction is obtained for λ as high as 1.99, obviously (see below), at such high value of λ, it is highly sensitive to initial guess, so our choice of initial guess becomes critical to get good reconstruction for such high values, here our initial guess is a square matrix with 0 23 as the value of each element Figures 5 9(a)-(h) are the corresponding reconstructions using MART 2 with initial guess as 0 21 and nearly similar results are observed

Figures 5 10(a)-(f) are the results using MART 3 The algorithm has failed to converge for λ>1.0, while rest of the reconstructions are similar to other MART algorithms

5.4 RECONSTRUCTION WITH DIFFERENT INITIAL FIELD VALUES

Reconstruction results for different initial field values are shown in figs 5 11(a)-5 11(d) For each of these reconstructions Simple ART has been used with λ fixed at 0 01 and e at 0 1 ART is an iterative technique and number of iterations to converge depends on initial field values, but final field should be nearly independent of initial guess, on using a fixed stopping criteria This is clearly evident from the reconstruction results On varying initial guess field from 0 to 1 0, it is found that the reconstruction is nearly same for all of them, except for fig 5 11(c) where $f'=0$ The number of iterations to converge for initial guess as zero are considerably lower than with other cases, and this can be the reason for the exception Table 5.1 lists the number of iterations to converge for different initial field values

S. No	Number of iterations (n)	Initial guess (f_i)
1	424	0.2
2	232	1
3	32	0
4	176	0.5

Table 5.1. Depicts Change in the number of iterations to converge
for different initial field values using simple ART

The combined effect of relaxation parameter and initial guess has been studied extensively, and the reconstruction is found to be nearly independent of initial guess for different values of relaxation parameter This is clearly evident from figs 5 12(a)-(b) that as the value of λ changes the independence is maintained as discussed above

The results using MART are in striking contrast to that from ART as the relationship between reconstruction and initial field value was affected by the value of relaxation parameter used Figures 5 13(a)-(d) are the reconstructions using MART1 It can be seen, that on changing λ from 0 1 to 0 5, the reconstruction is no longer independent of initial guess Similar results using MART 2 are shown in figs 5 14(a)-(d)

5.5 NUMERICAL SIMULATION

To check the performance of algorithms used above, the dataset is generated using a simulated specimen similar to the experimental object, i e a 30X30mm specimen with a circular central insert of diameter 6mm The reconstruction is carried out by considering weight matrix W_{ij}, obtained from straight-line assumption The slowness of the insert is taken as twice of base material The longitudinal velocity in the defect free region is taken as 30mm/μs The no. of views as well as the no of rays per view remain the same as used for experimental results. To be able to compare better with the experimental results the error levels are calculated for all the algorithms with different values of relaxation parameter The results are presented under the following subheadings The error EL1 and rms error EL2 for subsequent error analysis are as follows,

$$ EL1 = \frac{100}{N(f_{max} - f_{min})} \sum_{i=1}^{N} \left(\left| f_{original} - f_{reconstructed} \right| \right) \qquad (5\ 2) $$

$$ EL2 = \frac{\sqrt{\dfrac{\sum_{i=1}^{N}(f_{actual} - f_{reconstructed})^2}{N}}}{f_{max} - f_{min}} \times 100 \qquad (5\ 3) $$

5.5 1 Numerical Simulation using ART Algorithms

To be able to compare better with the experimental results the error levels are calculated for all algorithms used for different values of relaxation parameters

1. Simple ART

S No	EL1	EL2	λ	Iterations
1	11 32	16 53	1 99	401
2	11 33	14 8515	1 5	71
3	11 37	16 9	1 0	313
4	10 755	16 21	0 5	114
5	10 56	15 99	0 1	477
6	14 56	27 08	0 01	111
7	14 56	25 8	0 001	1198
8	661	1274 3	0 0001	224

Table-5 2 Different error levels, number of iterations, and relaxation parameters are given for the reconstruction of simulated specimen using Simple ART

Different error levels for a range of relaxation parameters are presented for Simple ART The algorithm doesn't seem to follow any particular dependence of error or number of iterations on λ. Minimum error levels are observed at $\lambda=0$ 1

2. Gordon ART

S No	EL1	EL2	λ	Iterations
1	8 19	10 74	1 99	54
2	10 61	15 76	1 5	61
3	10 56	15 72	1 0	74
4	10 61	15 786	0 5	570
5	9 71	14 85	0 1	186
6	12 99	22 04	0 01	129
7	20 82	47 06	0 001	465
8	91 61	361 82	0 0001	566

Table-5 3 Different error levels, number of iterations, and relaxation parameters are given for the reconstruction of simulated specimen using Gordon ART

Different error levels for a range of relaxation parameters are presented in table 5 3for Gordon ART It has shown better performance than Simple ART for all values of λ, with significant reduction in error levels The algorithm is most efficient in terms of number of iterations and error values for $\lambda=0$ 1

3. Gilbert ART

S No	EL1	EL2	λ	Iterations
1	85 62	87 23	0 5	4
2	12 23	19 9	0 1	15
3	12 16	19 86	0 01	158
4	29 82	80 92	0 001	258

Table-5.4 Different error levels, number of iterations, and relaxation parameters are given for the reconstruction of simulated specimen using Gilbert ART

Gilbert ART converged the problem only for relaxation parameters lesser than 0 5 and except for $\lambda=0$ 1 and $\lambda=0$ 01, the error values are too high

5.5 2   Numerical Simulation using MART Algorithms

1. MART 1

S No	EL1	EL2	λ	Iterations
1	0 9083	8 9665	1 99	5
2	21 59	27 57	1 5	3
3	39 97	41 54	0 5	3
4	9 56	14 21	0 1	15
5	10 41	15 876	0 01	118
6	26 159	77 808	0 001	169
7	68 68	353 33	0 0001	381

Table-5 5 Different error levels, number of iterations, and relaxation parameters are given for the reconstruction of simulated specimen using MART 1

MART 1 is different from the above ART algorithms in the sense that it has shown least error levels at such a high value of relaxation parameter with few iterations Also for $\lambda =0$ 1 the performance is better than ART algorithms

2. MART 2

S No	EL1	EL2	λ	Iterations
1	28 42	31 33	1 99	4
2	35 29	37 94	1 5	9
3	87 93	88 62	0 5	17
4	8 42	13 42	0 1	36
5	11 28	19 93	0 01	136
6	50 29	172 83	0 001	138
7	665 56	3221 3	0 0001	77

Table-5.6 Different error levels, number of iterations, and relaxation parameters are given for the reconstruction of simulated specimen using MART 2

Different error levels for a range of relaxation parameters are presented in Table 5 6 for MART 2 The algorithm is most efficient in terms of number of iterations and error values for λ=0 1 and also has the least error level for λ=0 1 among the additive and multiplicative category

3. *MART 3*

S No	EL1	EL2	λ	Iterations
1	9 25	13 66	0 1	18
2	13 17	16 06	0 01	40
3	17 95	21 81	0 001	140
4	102 63	404 12	0 0001	79

Table-5 7 Different error levels, number of iterations, and relaxation parameters are given for the reconstruction of simulated specimen using MART 3

MART 3 failed to converge for relaxation values more than 0 1 and have shown best rms EL2 and EL1 for λ=0 1

Errors due to reconstructions for these six algorithms are presented The best value of relaxation parameter that gives minimum error and fastest convergence has been determined through numerical experimentation and has been reported for the ART and MART algorithms

High value of EL1 and EL2 for these algorithms can be attributed to limited number of views, in this case 4 views Increasing the number of views generally decreases rms error and error as low as 2 0 is reported for 8 views It is remained as such to be able to compare better with the experimental results Gilbert ART have shown largest RMS error In ART family, Gordon ART has shown best results for this problem

MART algorithms have shown less error (EL1 as well as EL2) than ART family for 0 01 ≤ λ ≤ 0 1 Particularly, MART 2 has shown best performance at λ=0 1 in the additive and multiplicative family of algorithms

5.6 SIMULATED RESULTS

Simulated Specimen
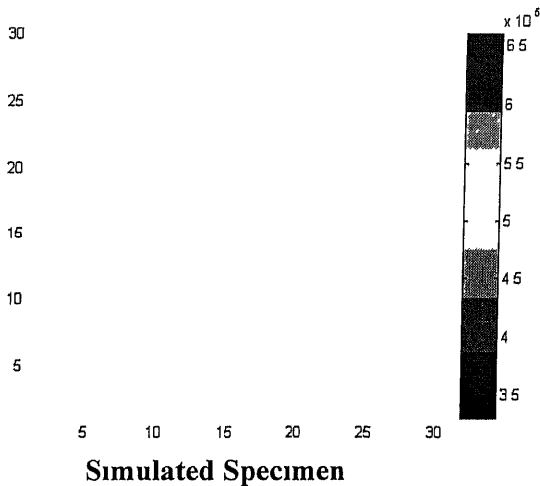
Here, simulation is performed to check the performance of the algorithms used Figure 5 15 to 5 20 are the results obtained after reconstruction The reconstructions using MART1 and MART2 are better than other algorithms as expected from their RMS values, so these two algorithms are shortlisted for further analysis

5.7 REVIEW OF EXPERIMENTAL RESULTS BASED ON SIMULATED STUDY

The superimposition of experimental results with the simulated study clears the factor of algorithm dependency on confusion of image interpretation, so that physical reasons can be ascertained to deviations from the examined body The experimental results are again discussed to fix some of the suspicions MART1 and MART2 are used for their better performance as discussed above for $\lambda = 0\ 1$

The lines at 45 and 135 degrees in the experimental result can now be ascertained to the directional dependence or anisotropy in the base material, as the result of application of anisotropic algorithm on an anisotropic material Similar results for 0 and 90^0 affirms the cross ply arrangement of fabric

As can be seen from the results (Fig 5 21 to fig 5 24) that it can generate defect location and geometry The size of the defect is somewhat large, though not far away from the actual values The reason can be attributed to the bending of ray near the edge of the flaw, which is not accounted for in the straight line assumption

5.8 POSSIBLE SOURCES OF ERROR

The data acquired from laser based Ultrasonics (LBU) setup are for limited views and few number of rays per view, so the following sources of errors are inevitable

1   Experimental error
- Location
  Fine manual adjustments are required to fix the position of sources and receivers to the marked points and the inaccuracies in positioning may result in error in subsequent reconstruction
- Time Of Flight (TOF)
  There may be some error in taking the Time Of Flight (TOF) value from the A-scan images

2   Incomplete data
  Linear interpolation has been used to fix the in between projections and this may be one of the sources of error

5.9 Closure

In this chapter, the Time Of Flight (TOF) information from the A- Scan images has been obtained from Laser-Based Ultrasonic (LBU) set-up and subsequently reconstructed the slowness values for the domain under consideration using different ART and MART algorithms for different values of relaxation parameter and initial guesses and compared the results with numerical simulation
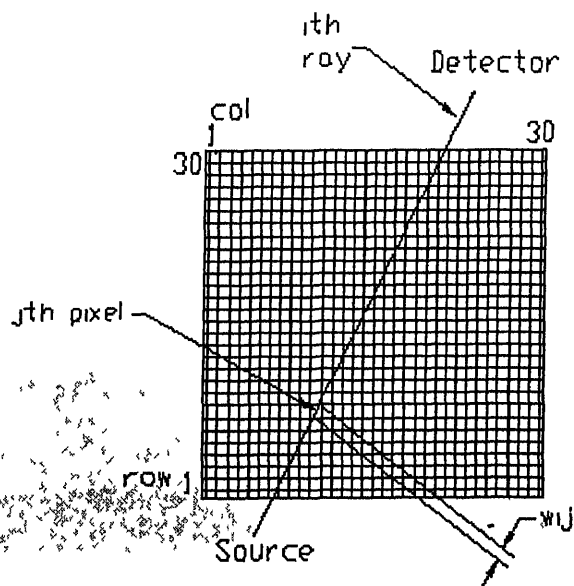
fig. 5.1(o) Discretization of object plane
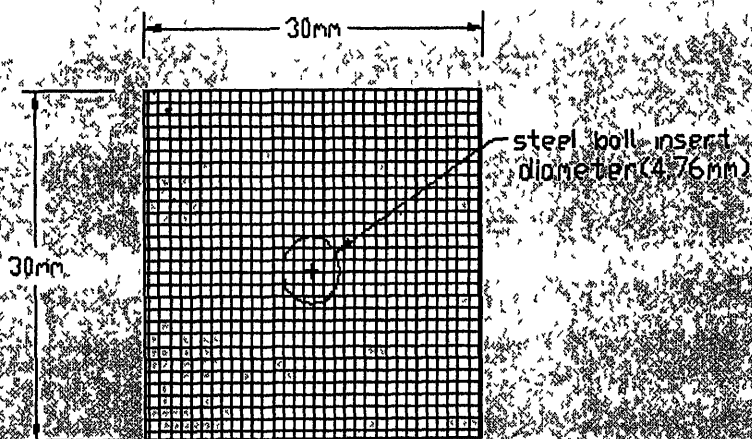
fig. 5.1(b) Schematic view of the domain under consideration

Y-Axis

30 nm

4.76 mm
+

source
positions

reciever
positions
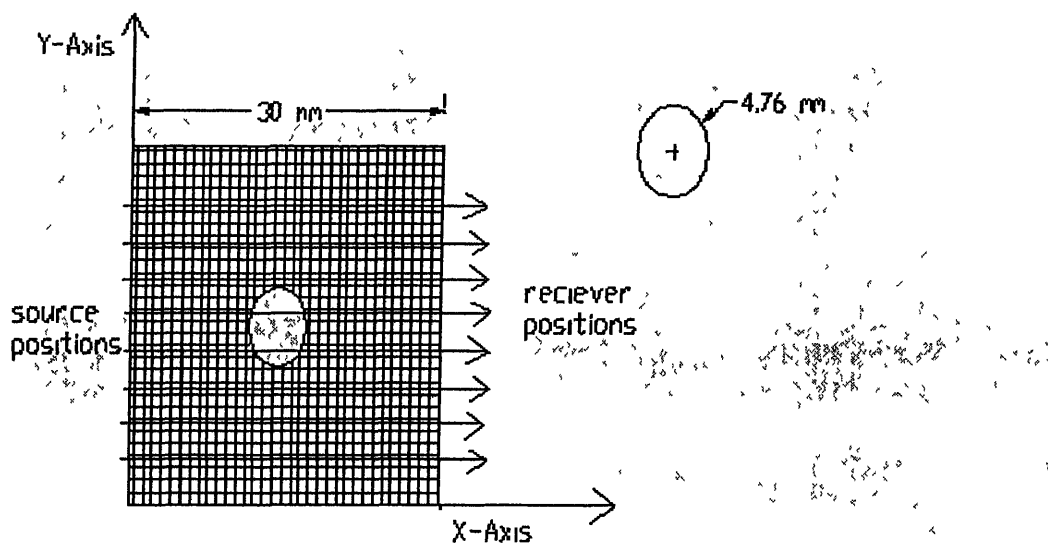
X-Axis

fig. 51(c) Rays at 0° along X-Axis

reciever
positions

4.76 mm
+

Y-Axis

30 nm

source
positions

X-Axis
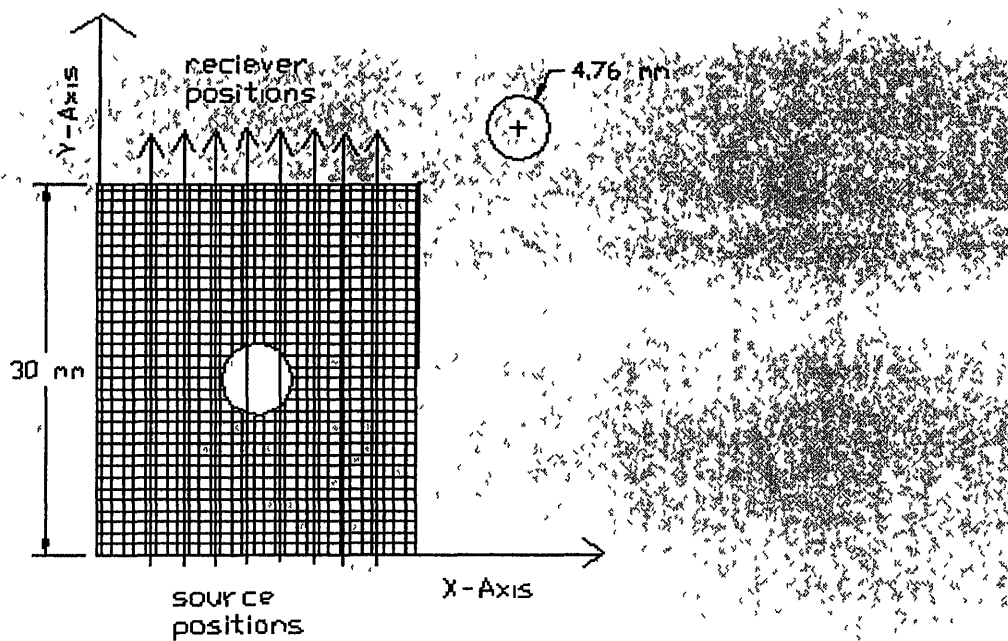
fig 51(d) Rays at 90° along Y-Axis

Y-Axis

Reciever positions

—476 mm

source
positions

30 mm

x-Axis

fig. 5.1(e)   Roys at 45°

Y-Axis   Source
Positions

X-Axis

30 mm

Reciever
Positions

—476nn

fig. 51(f) Roys at 135°
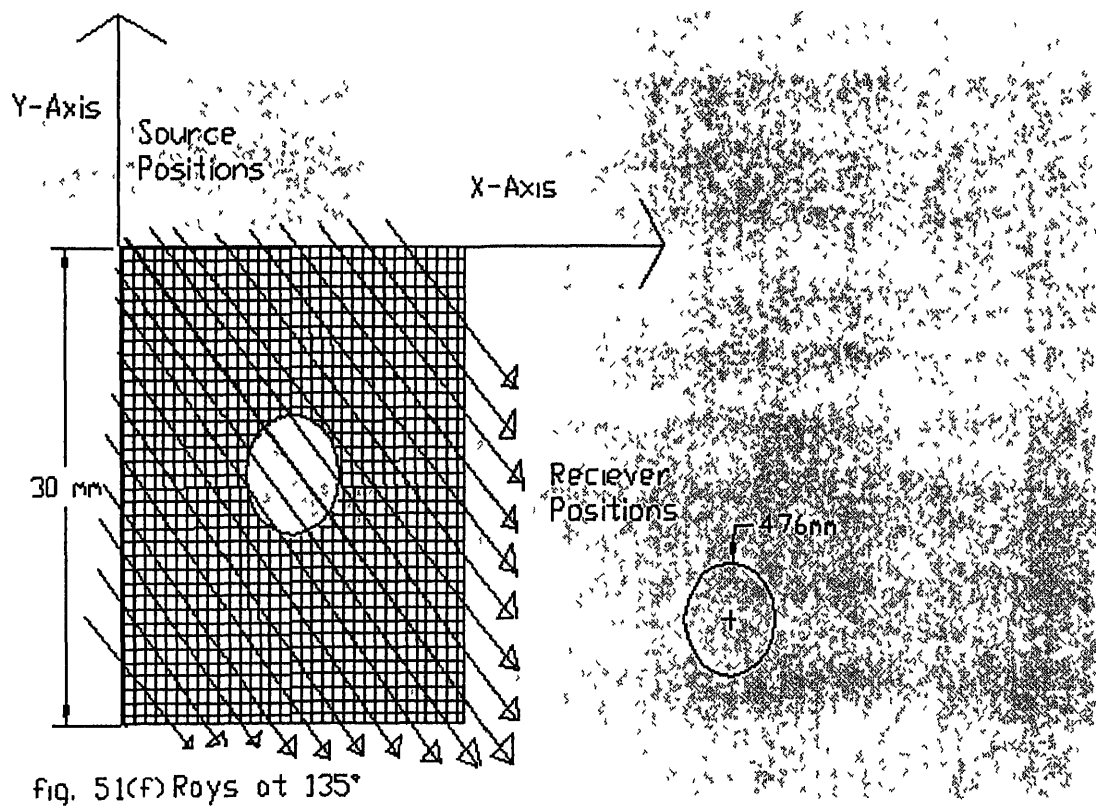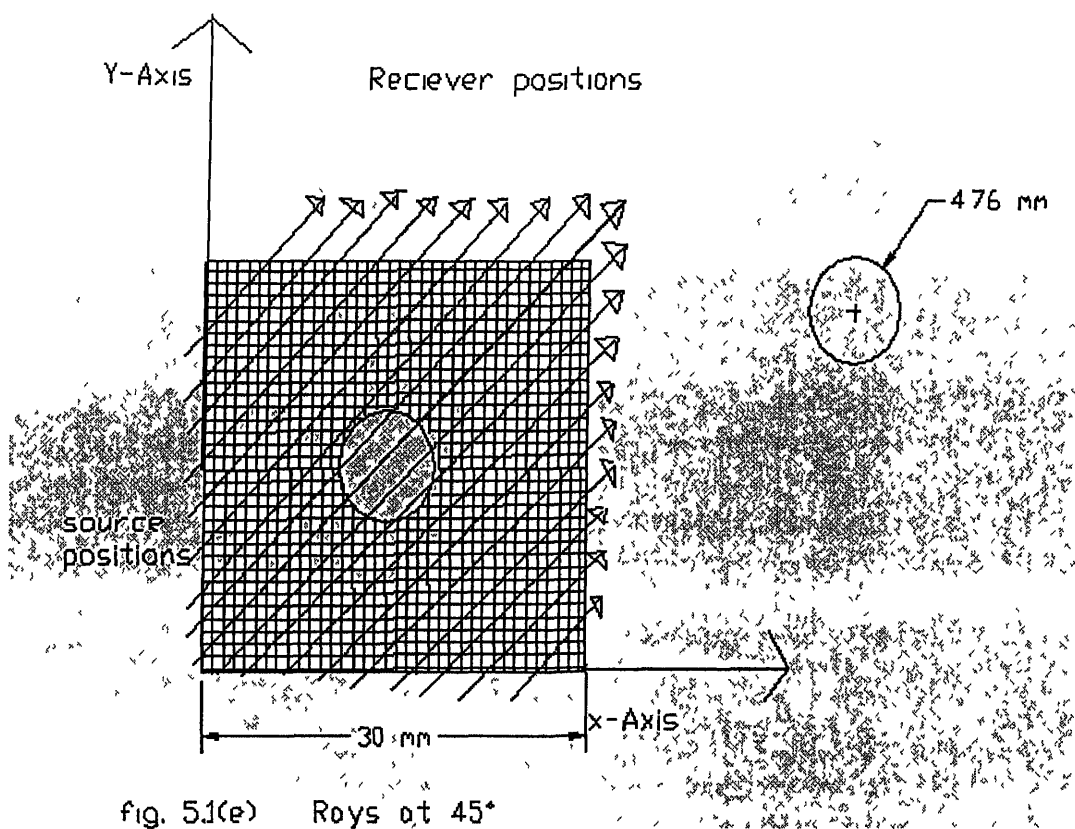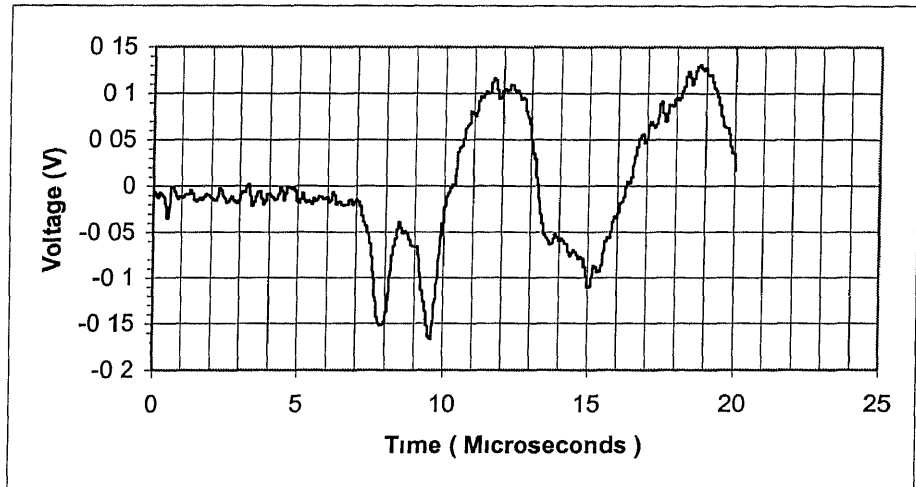
Case 1 - Input at 5th column
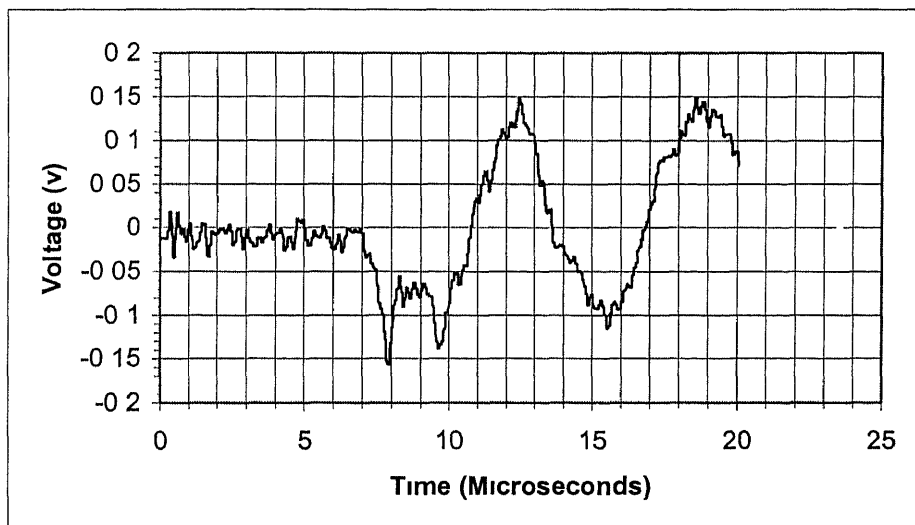
Case 2 - Input at 14th column

Figure 5 3 Signal at the receiver end due to excitation along 90^0 (Y-direction)
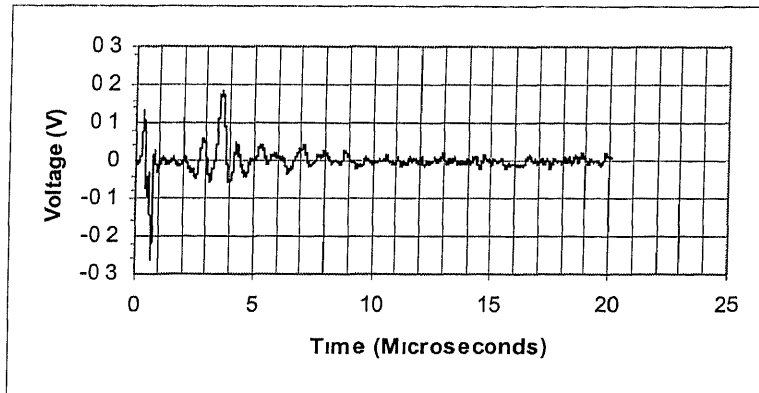
Case - 1 Time of Flight (2 2 μs)
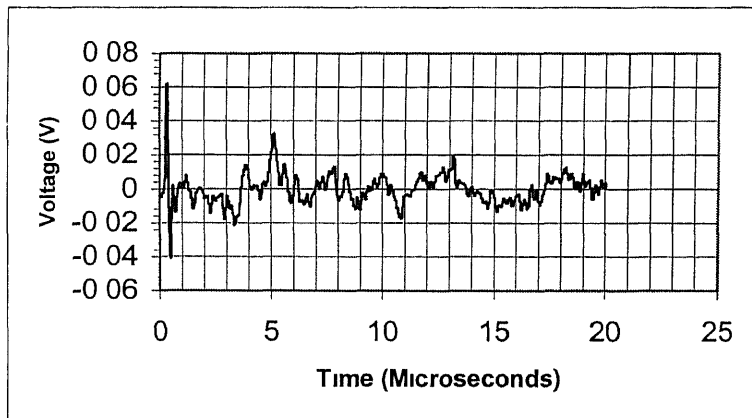
Case - 2 Time of Flight (3 4 μs)
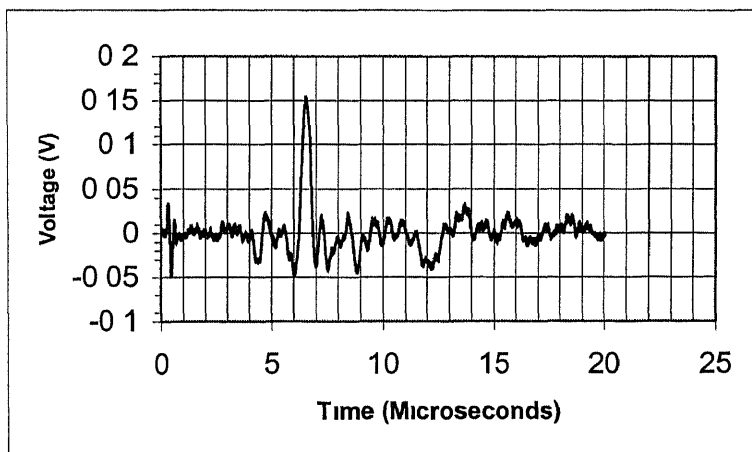
Case - 3 Time of Flight (4 0 μs)
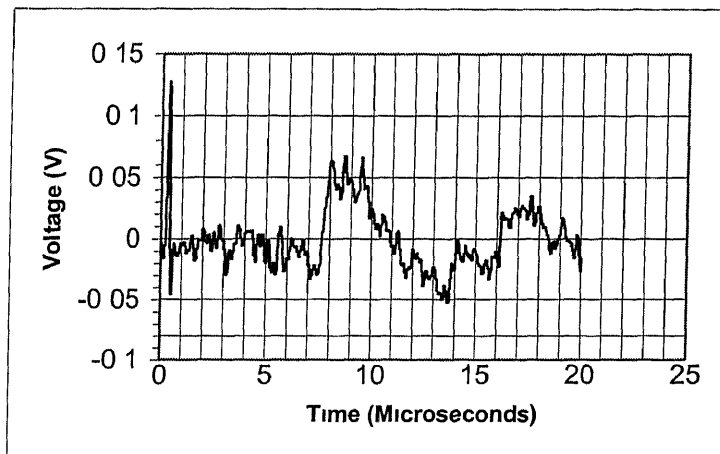
Case - 4 Time of Flight (7 4 µs)
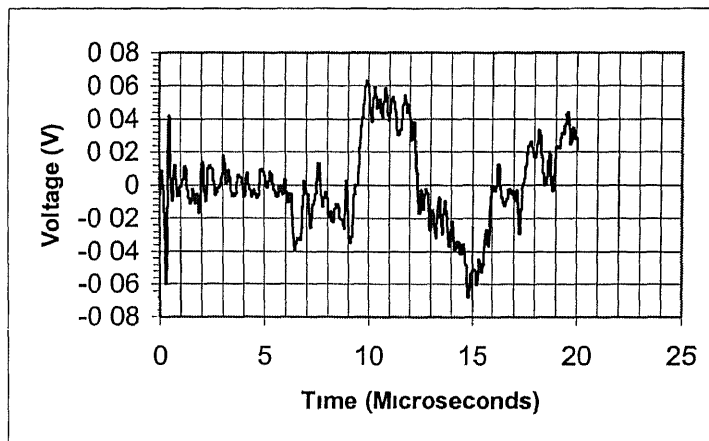
Case - 5 Time of Flight (9 0 µs)
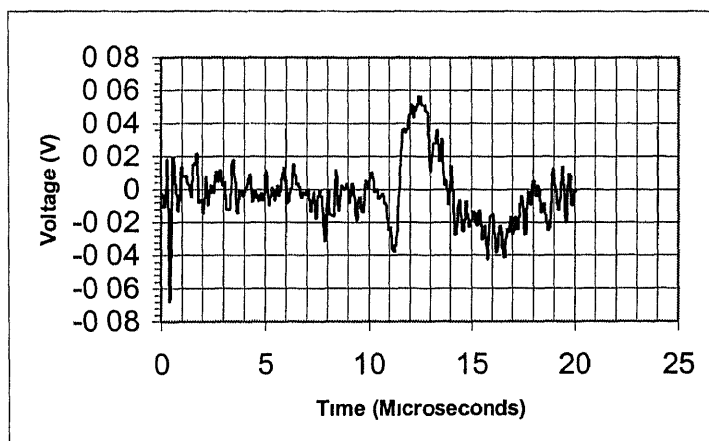
Case - 6 Time of Flight (10 8 µs)
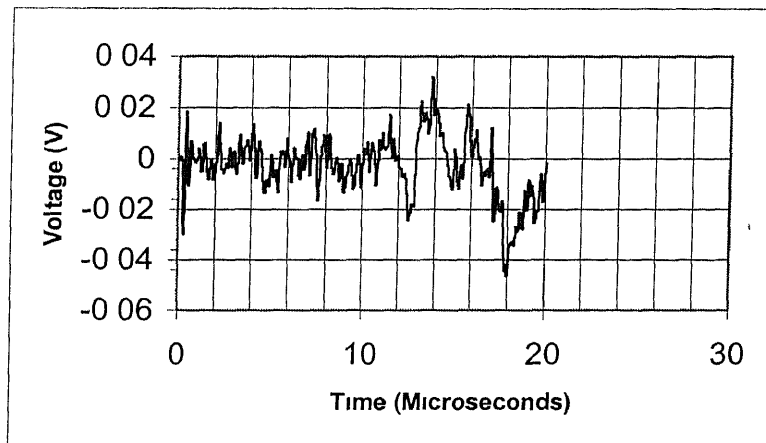
Case - 7 Time of Flight (12 2 μs)
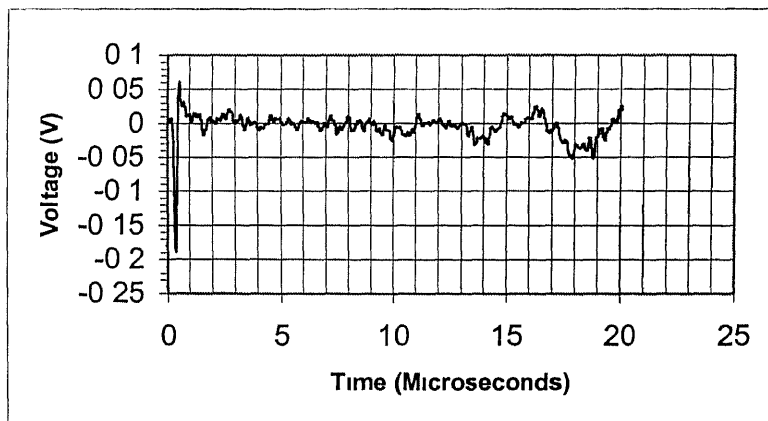
Case - 8 Time of Flight (14 0 μs)
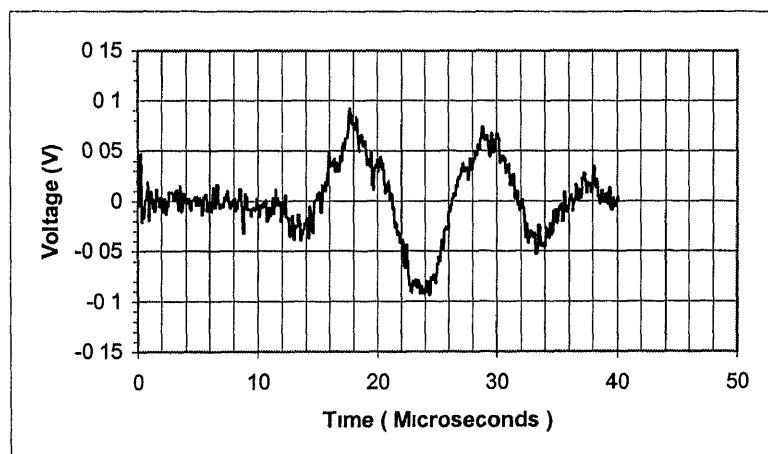
Case - 9 Time of Flight (17 5 μs)

Figure 5 4 Signal at the receiver end due to excitation along 45^0 wrt X-axis
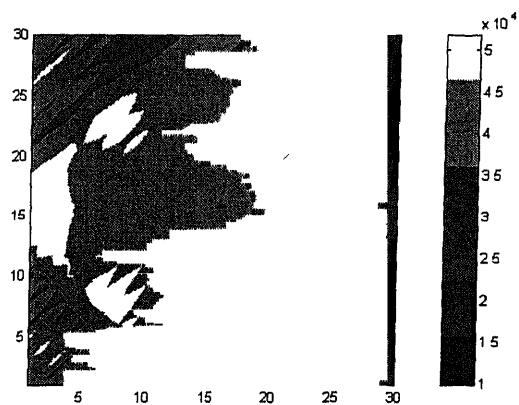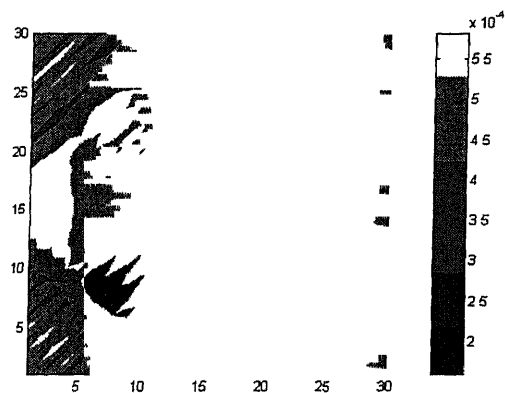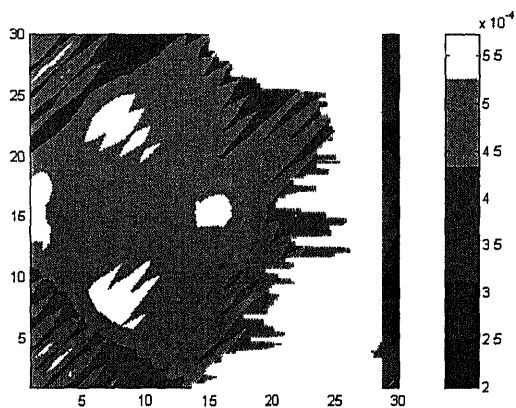
Fıgure 5 5(a) λ=1.99

Fıgure 5.5(b) λ=1.5

Fıgure 5 5(c)· λ=1.0

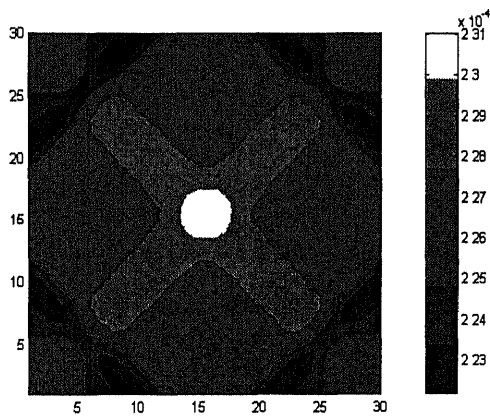

Fıgure 5 5(d)· λ=0.5
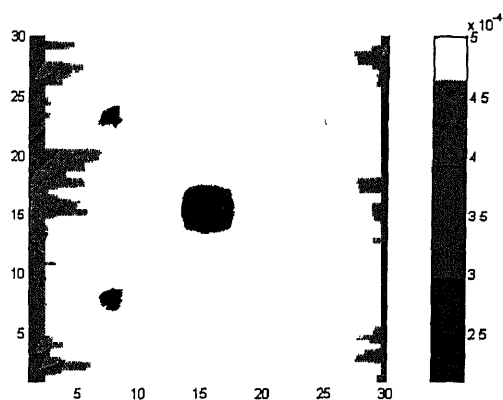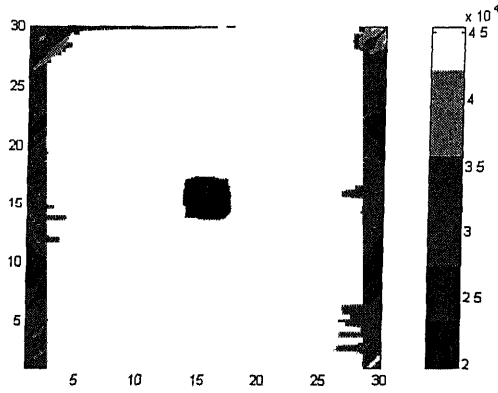
Figure 5 5(e)· λ=0.1
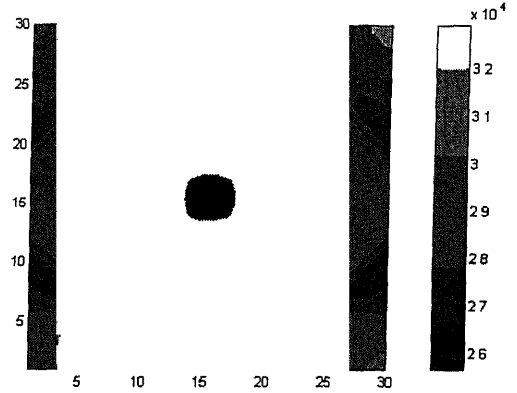
Figure 5 5(f): λ=0.01
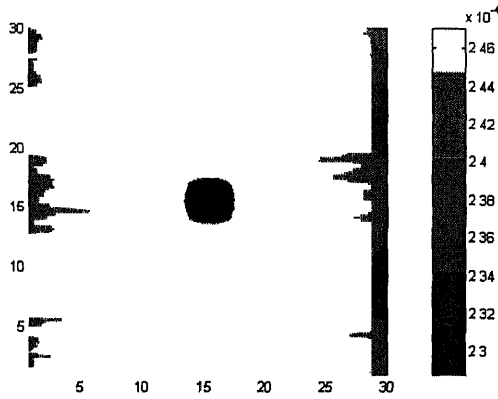
Figure 5.5(g): λ=0.001
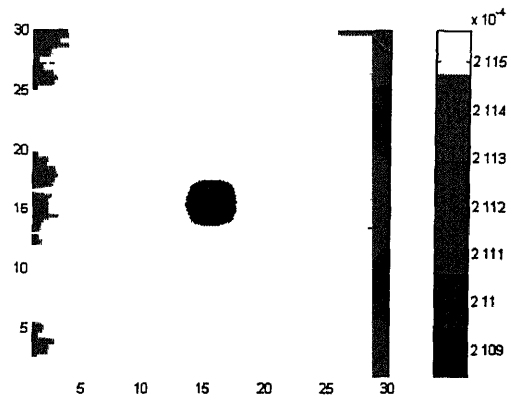
Figure 5.5(h): λ=0.0001

Figure 5.5(a)-5.5(h): Reconstruction of slowness values for different relaxation parameters using Simple ART (Material: Glass/epoxy with central steel insert)
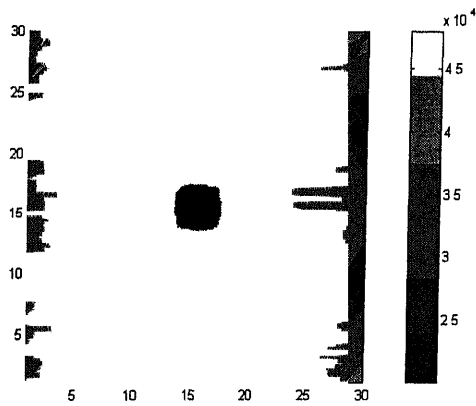
Figure 5 6(a) λ=0 1
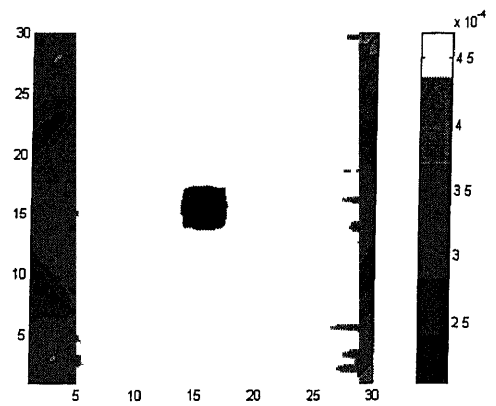
Figure 5.6(b). λ=0.01
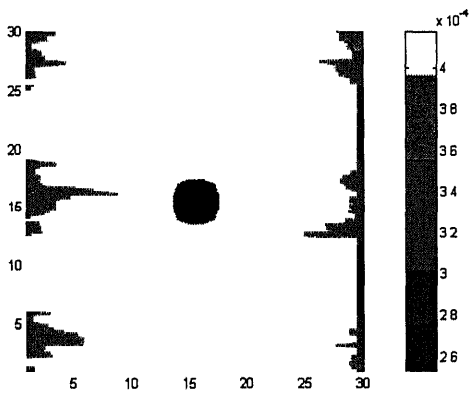
Figure 5.6(c): λ=0.001
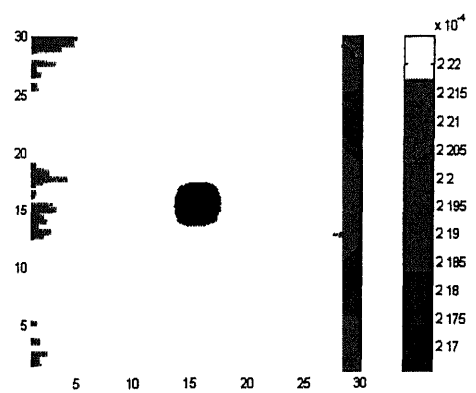
Figure 5.6(d). λ=0.0001

Figure 5.6(a)-5.6(d): Reconstruction of slowness values for different relaxation parameters using Gordon ART (Material: Glass/epoxy with central steel insert)
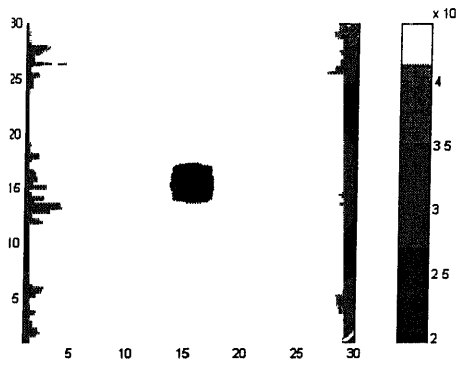
Figure 5.7(a) λ=0.1
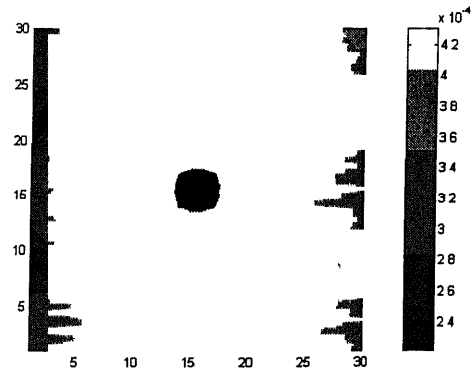
Figure 5.7(b) λ=0 01
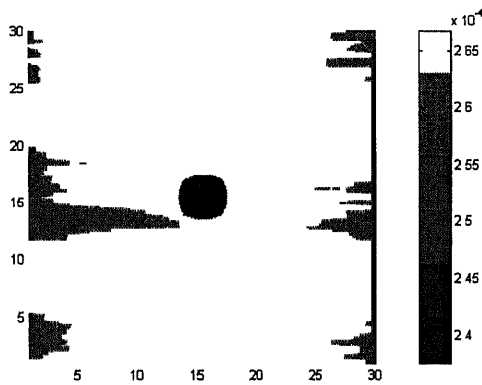
Figure 5 7(c) λ=0 001
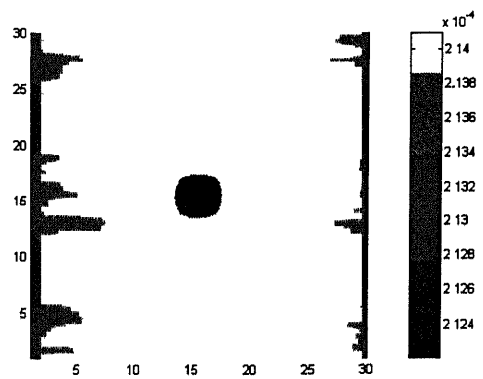
Figure 5.7(d) λ=0.0001

Figure 5.7(a)-5.7(d). Reconstruction of slowness values for different relaxation parameters using Gilbert ART (Material. Glass/epoxy with central steel insert)
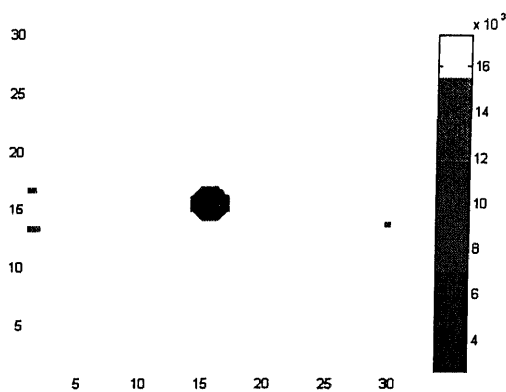
Figure 5.8(a): λ=1.99
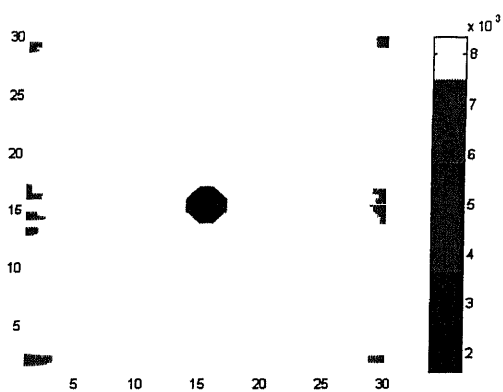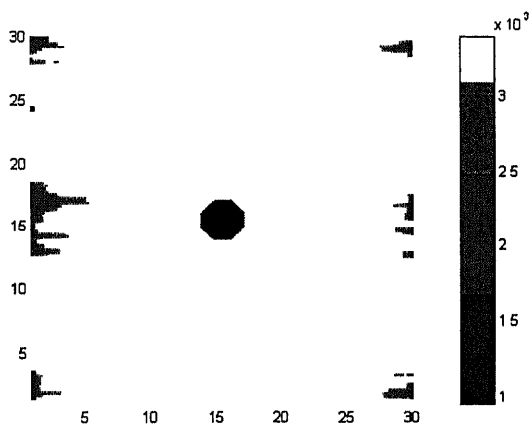
Figure 5 8(b): λ=1.5

Figure 5.8(c): λ=1 0
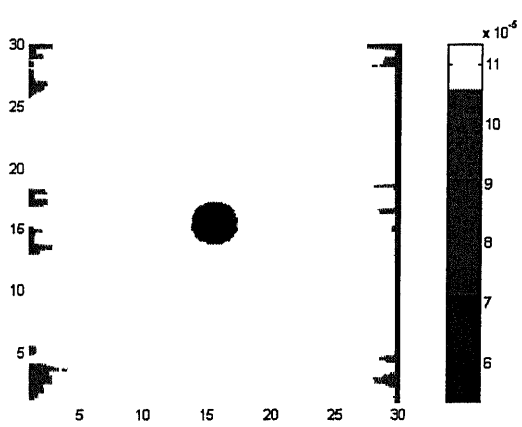
Figure 5.8(d): λ=0.5
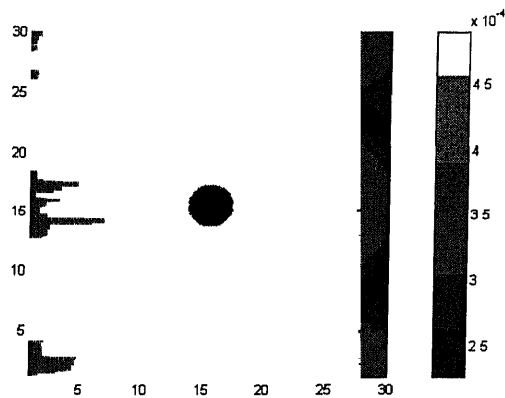
Figure 5.8(e) λ=0.1
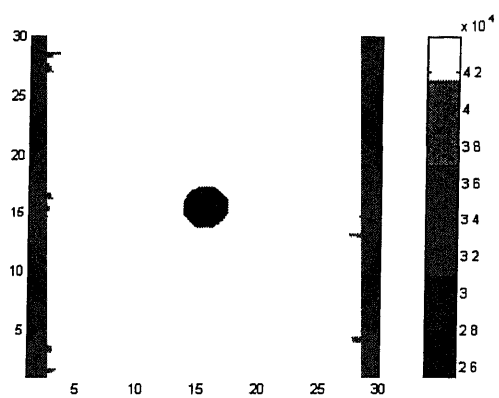
Figure 5.8(f)· λ=0.01
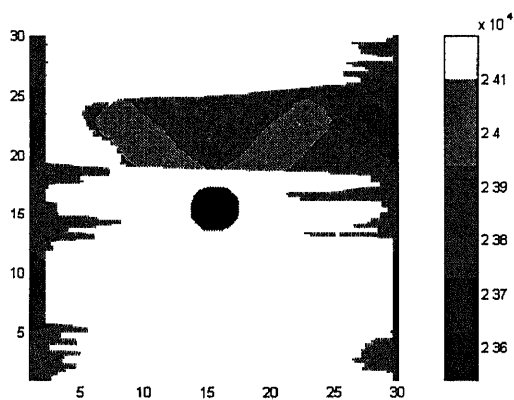
Figure 5 8(g). λ=0.001
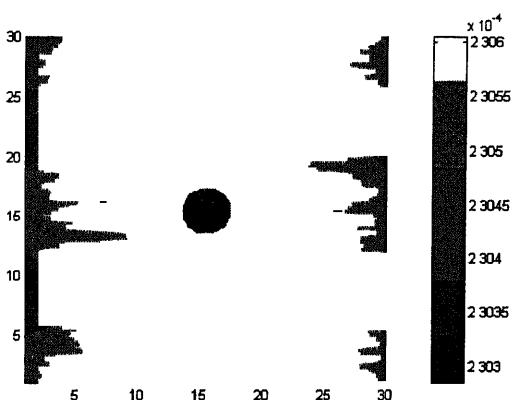
Figure 5.8(h): λ=0.0001

Figure 5.8(a)-5.8(h)· Reconstruction of slowness values for different relaxation parameters using MART 1 with f^t =0.23 (Material. Glass/epoxy with central steel insert)
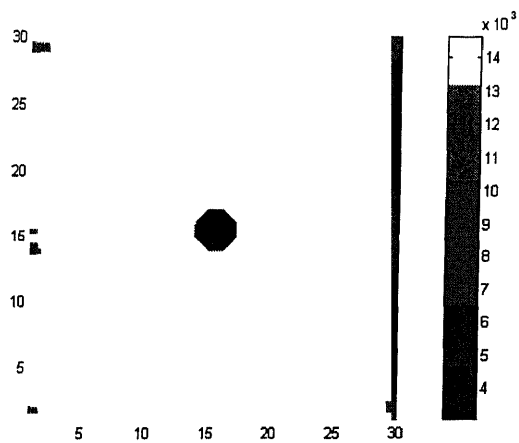
Figure 5.9(a). λ=1.99
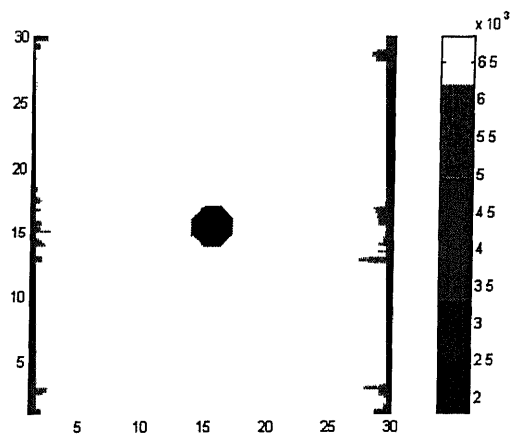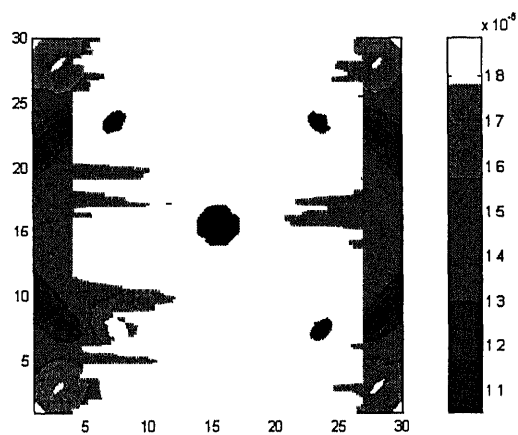
Figure 5 9(b): λ=1.5

Figure 5.9(c): λ=1 0
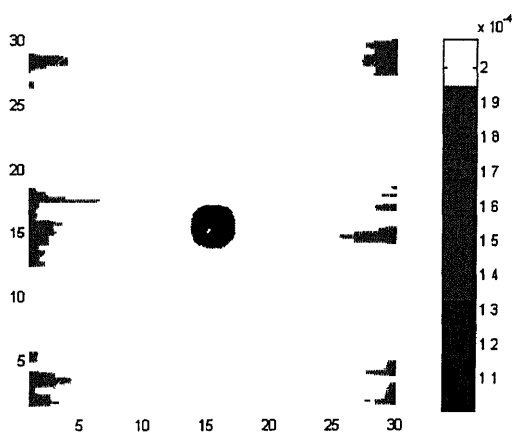
Figure 5.9(d)· λ=0.5
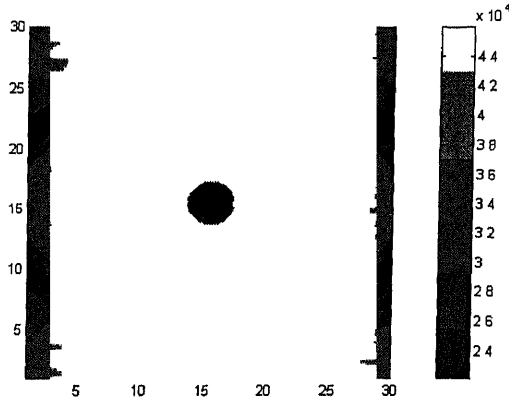
Figure 5.9(e)· λ=0.1
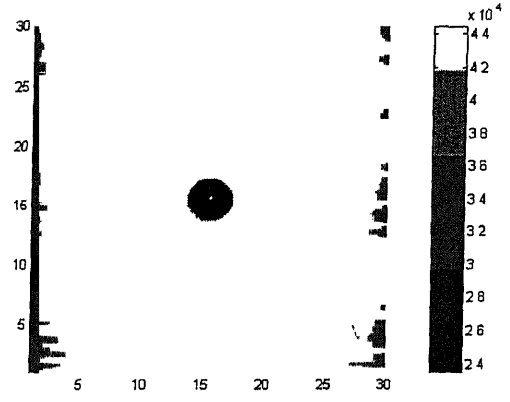
Figure 5.9(f) λ=0 01
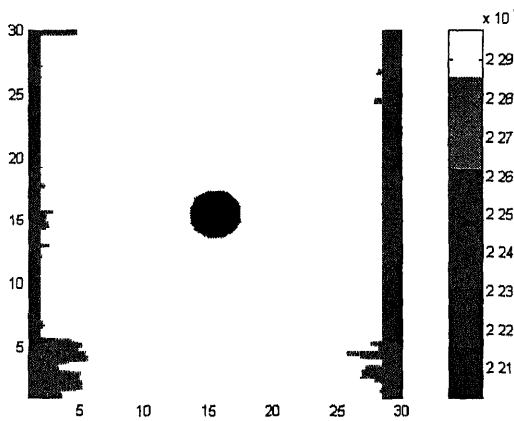
Figure 5.9(g)· λ=0.001
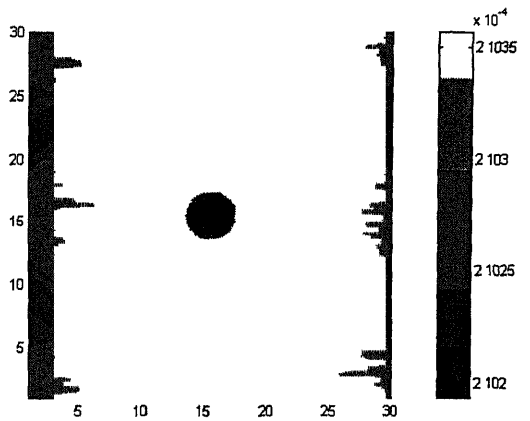
Figure 5 9(h): λ=0.0001

Figure 5.9(a)-5.9(h). Reconstruction of slowness values for different relaxation parameters using MART 2 with f' =0.21 (Material: Glass/epoxy with central steel insert)
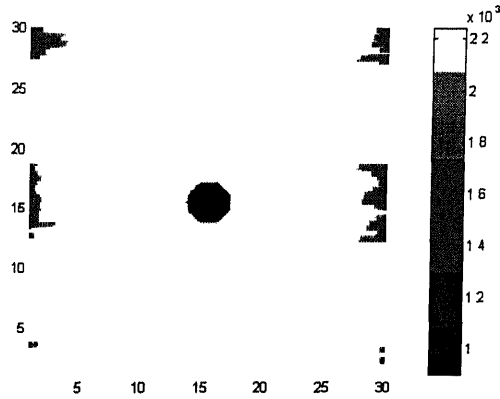
Figure 5.10(a): λ=1.0
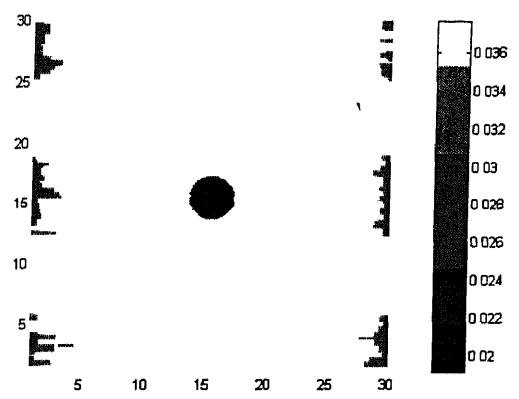
Figure 5.10(b): λ=0 5
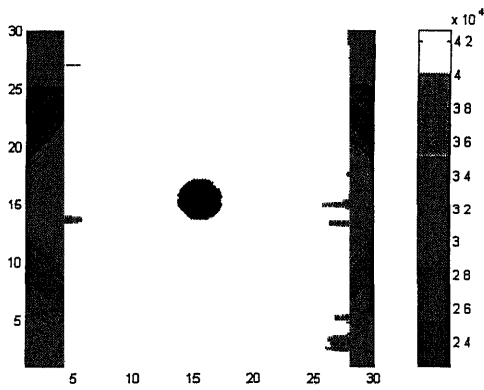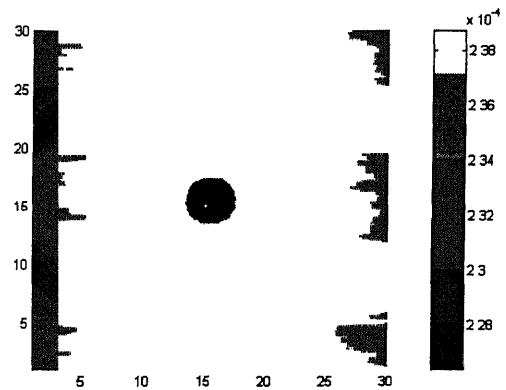
Figure 5.10(c). λ=0.1

Figure 5.10(d). λ=0.01

Figure 5.10(e): λ=0 001
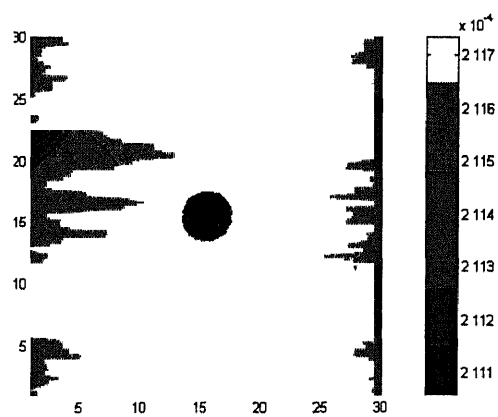
Figure 5 10(f) λ=0 0001

Figure 5.10(a)-5.10(f): Reconstruction of slowness values for different relaxation parameters using MART 3 with f^i =0.21 (Material: Glass/epoxy with central steel insert)
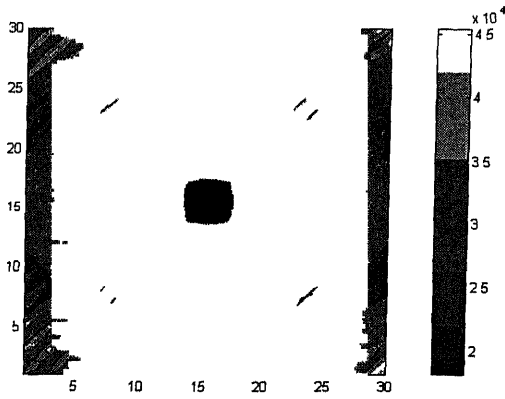
Figure 5 11(a). f^i=0 2
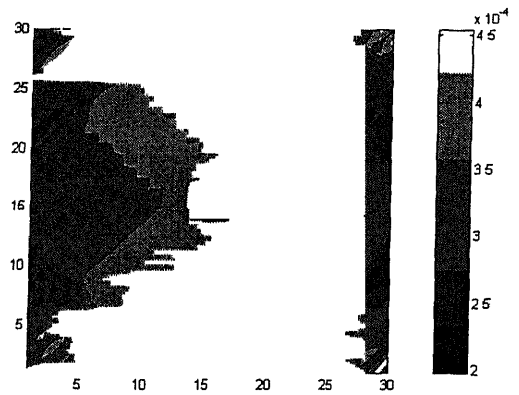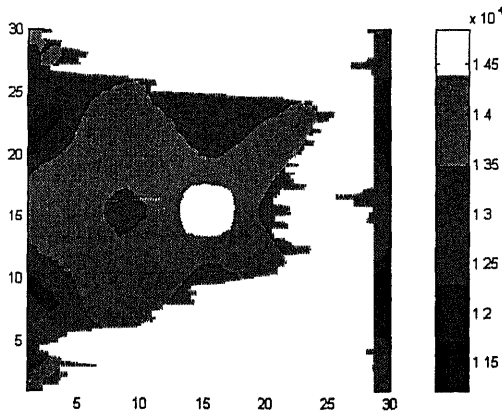
Figure 5.11(b): f^i=1
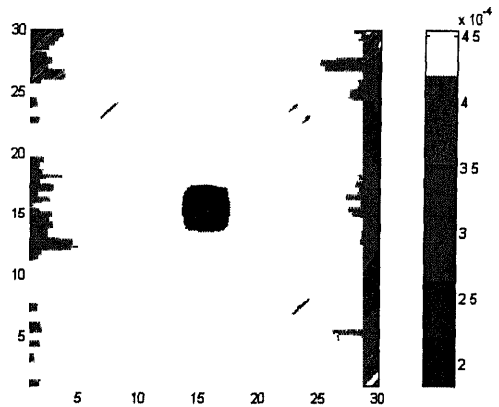
Figure 5.11(c): f^i=0

Figure 5.11(d): f^i=0 5

Figure 5.11(a)-5.11(d): Reconstruction of slowness values for different initial guess (λ =0.1, is same for all the cases). Material is Glass/epoxy with central steel insert
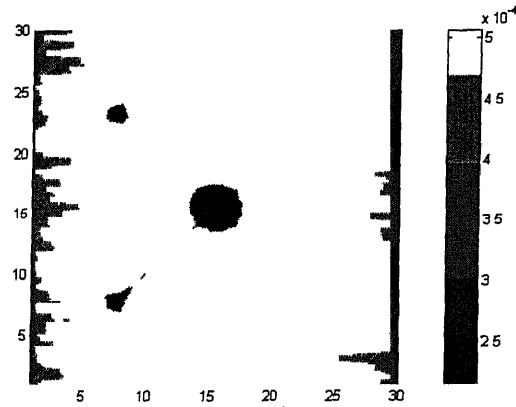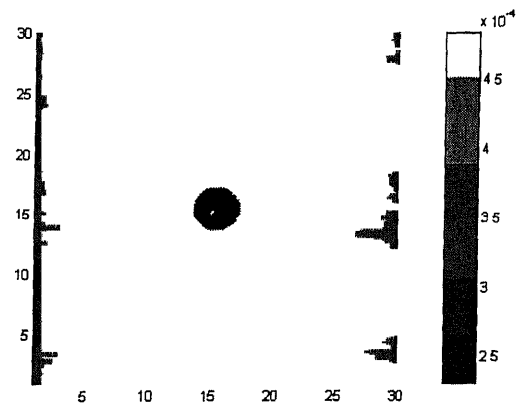
Figure 5.12(a). f^i=0 1
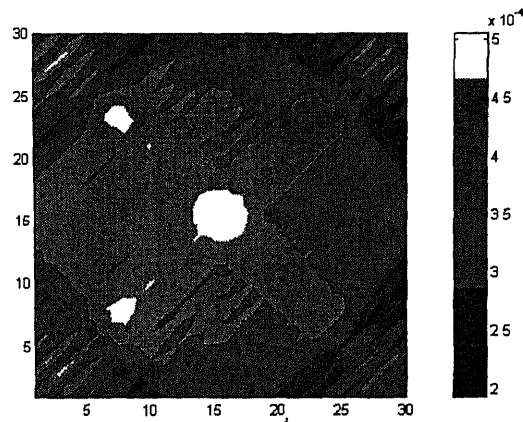
Figure 5.12(b) f^i=0.21

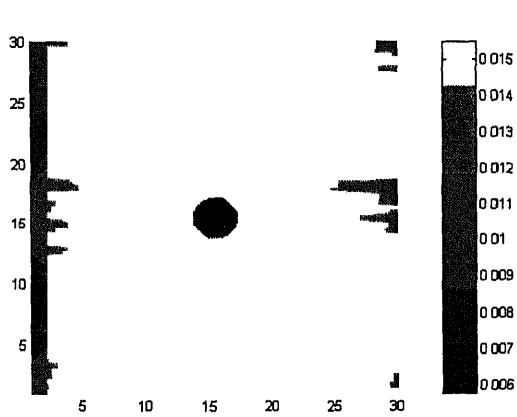Figure 5.12(a)-5.12(b): Reconstruction of slowness values for different initial guess (λ =0.5, is same for all the cases) Material is Glass/epoxy with central steel insert.
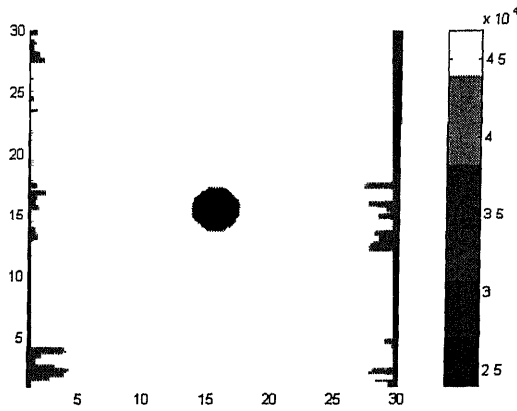
Figure 5 13(a) f^i=0 21, λ=0 1

Figure 5 13(b) f^i=0.1, λ=0 1

Figure 5.13(c)· f^i=0 1, λ=0.5
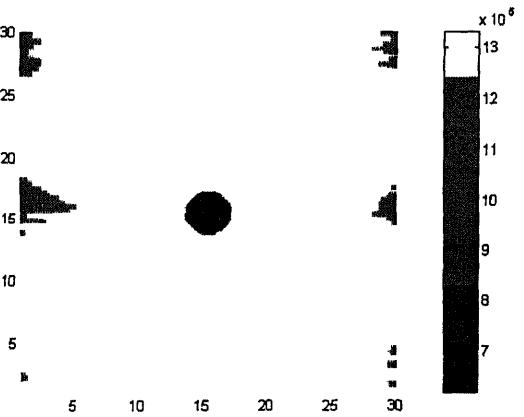
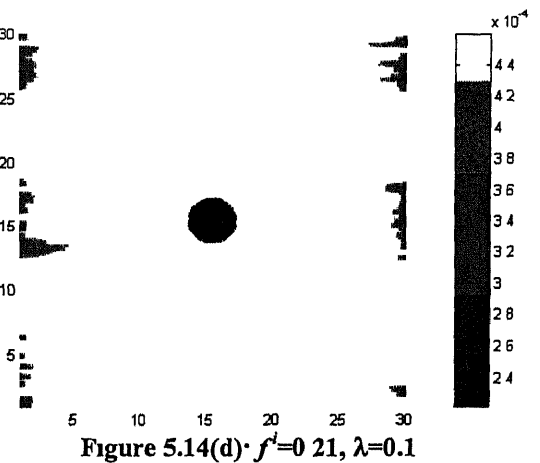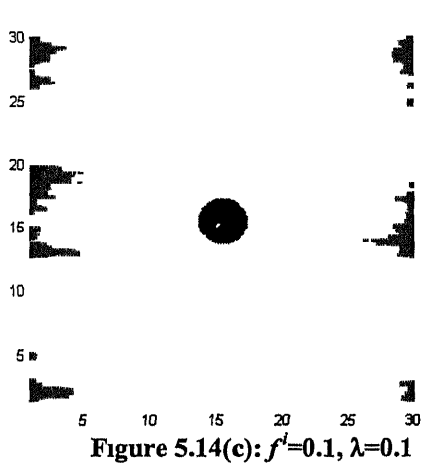Figure 5.13(d): f^i=0.21, λ=0.5

Figure 5.13(a)-(d) Depicting the combined effect of initial guess and relaxation parameter on reconstruction, using MART 1.

Figure 5 14(a)· f^i=0 1, λ=0.5

Figure 5.14(b): f^i=0.21, λ=0 5

Figure 5.14(c): f^i=0.1, λ=0.1
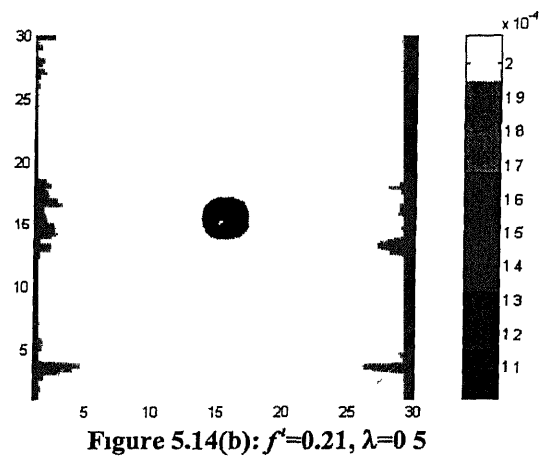
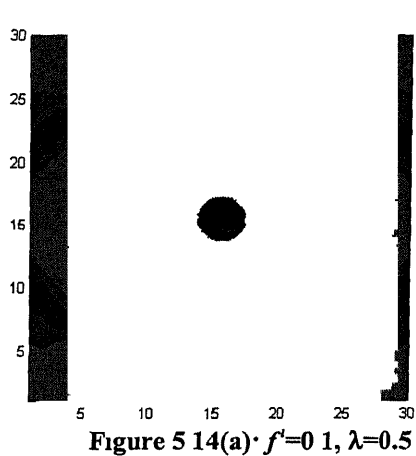Figure 5.14(d)· f^i=0 21, λ=0.1

Figure 5.14(a)-(d) Depicting the combined effect of initial guess and relaxation parameter on reconstruction, using MART 2.
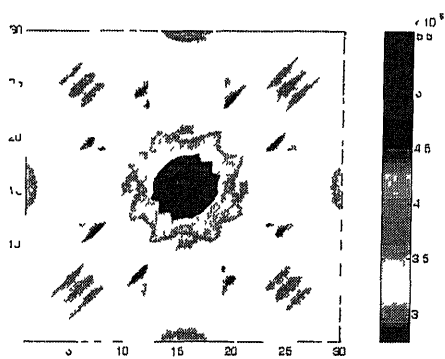
Fig 5 15 Reconstruction using Simple ART
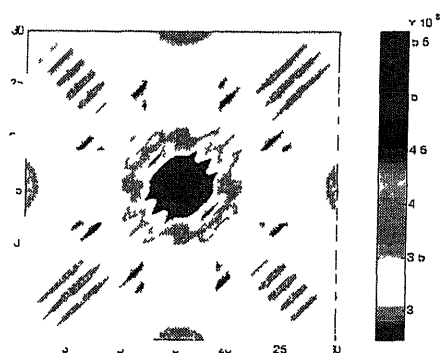(30 rays, 4 views, $\lambda = 0 1$)

Fig 5 16 Reconstruction using Gordon ART
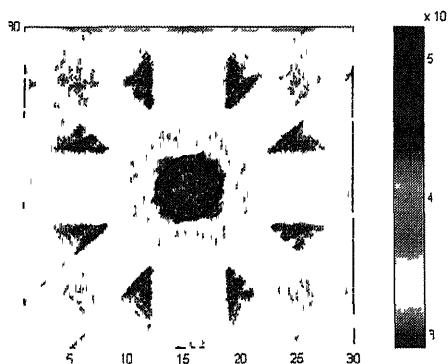(30 rays, 4 views, $\lambda = 0 1$)

Fig 5 17 Reconstruction using Gibert ART
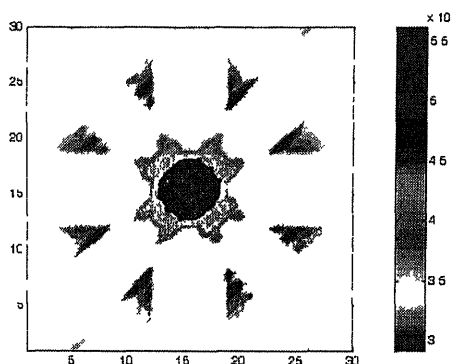(30 rays, 4 views, $\lambda = 0 1$)

Fig 5 18 Reconstruction using MART1
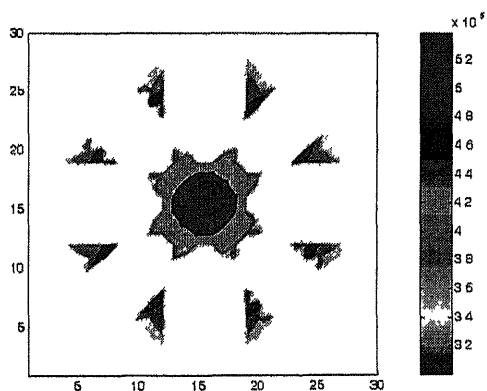(30 rays, 4 views, $\lambda = 0 1$)

Fig 5 19 Reconstruction using MART2
(30 rays, 4 views, $\lambda = 0 1$)
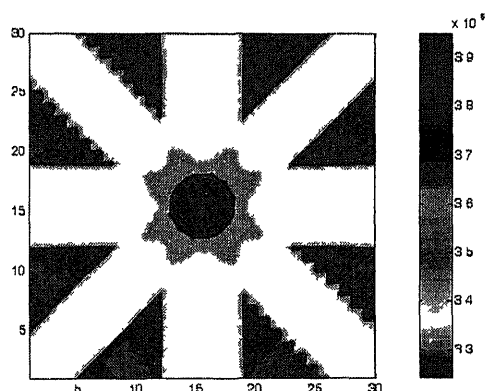

Fig 5 20 Reconstruction using MART3
(30 rays, 4 views, $\lambda = 0 1$)

Fig 5 21 Reconstruction using MART1
(**30 rays, 4 views,** $\lambda = 0\ 1$)

Fig 5 22 Reconstruction using MART1
(**30 rays, 4 views,** $\lambda = 0\ 1$)

Fig 5 23 Reconstruction using MART2
(**30 rays, 4 views,** $\lambda = 0\ 1$)

Fig 5 24 Reconstruction using MART2
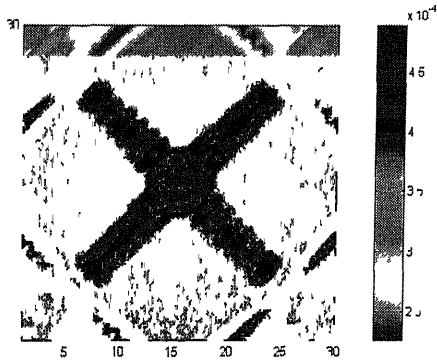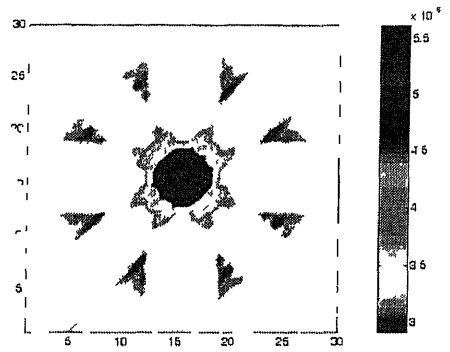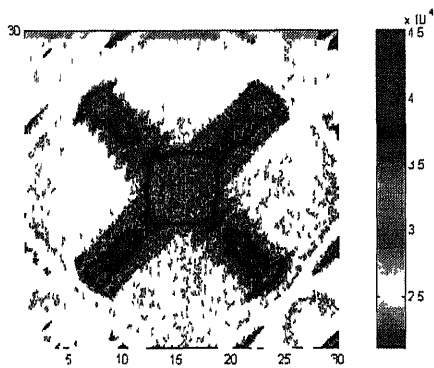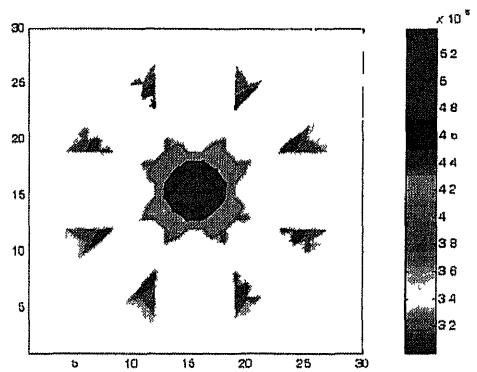(**30 rays, 4 views,** $\lambda = 0\ 1$)

Chapter 6
CONCLUSIONS AND SCOPE FOR FUTURE WORK

6.1 CONCLUSIONS

In the present study of tomographic reconstruction of defects in composite materials, most of the ART and MART algorithms are used for reconstruction and thereafter the results are compared with simulated reconstructions Laser based ultrasonic setup is used to find the time of flight data Based on the results obtained, the following conclusions are drawn

(1) Carefully obtained Time Of Flight (TOF) data from Laser based ultrasonic (LBU) setup is sufficient and satisfactory enough to be used for further Non-Destructive analysis

(2) The Algorithms (ART and MART) used here, neglecting ray bending, is capable to generate defect location and geometry The size of the defect may come somewhat larger than the actual value

(3) The reconstruction is found to be nearly independent of the initial guess value, which indicates the considerable insensitivity of the Algorithms to initial approximation, except for MART, when high values of relaxation parameter were used

(4) MART algorithms, especially MART 2 shows better performance than additive algorithms

(5) All the additive and multiplicative algorithms we discussed had shown less rms error for $\lambda=0$ 1, hence making it the preferred relaxation parameter for these algorithms

(6) The superimposition of simulation study on experimental results can enhance our confidence over the anisotropy in object

(7) Finally, the straight ray approximation and linear-interpolation, being oversimplifications, have not interfered with the accuracy of reconstruction to an extent, which may demand necessary incorporation of complexities

6.2 SCOPE FOR FUTURE WORK

(1) The time of flight data obtained from shear waves can be used for finding the defects in composite materials

(2) Experimental determination of shear waves is possible by making some changes in the interferometry

(3) Non-linear interpolation can be used to complete the data set

(4) Algorithms such as Maximum Entropy and Minimum Energy can be tried for reconstruction

References

[1] Krautkramer J and Krautkramer H "*Ultrasonic Testing of Materials*", 4th edition Springer-Verlag, New York, 1990

[2] Neshoth J B, Rose J L, Bashyam M and Subramanian K "Physically based ultrasonic feature mapping for anomaly classification in composite materials", *Materials Evaluation*, 1985, Vol 43, pp 541-546

[3] Rose J L "Elements of a feature-based ultrasonic inspection system", *Materials Evaluation*, 1984, Vol 42, pp. 210-218

[4] Sarin P.S "Development of laser-based ultrasonic Non-destructive testing", *M Tech Thesis*, January 2002, Department of Mechanical Engineering, Indian Institute of Technology, Kanpur.

[5] Daliraju G. "Experimental characterization of laser-based ultrasonic system", *M Tech Thesis*, February 2002, Department of Mechanical Engineering, Indian Institute of Technology, Kanpur.

[6] Scruby C.B. and Drain L.E. "*Laser Ultrasonics Techniques and Applications*", Adam Hilger Bristol, Philadelphia, New York, 1990.

[7] Kline R.A. "Ultrasonic computed tomography for anisotropic materials characterization", Ultrasonic Symposium, 1993

[8] Kline R. A., and Wang Y. Q. "A technique for ultrasonic tomography in anisotropic media", Journal of Acoustical Society of America, 1992, Vol 91, pp 878-884

[9] Kline R.A., Wang Y. Q., Mignogna R B. and Delsanto P O "A finite difference approach to acoustic tomography in anisotropic media", Journal of Nondestructive Evaluation, 1994, Vol. 13, No. 2, pp 75-83.

[10] Chow T. M., Hutchins D.A., and Mottram J T "Simultaneous acoustic emission and ultrasonic tomographic imaging in anisotropic polymer composite material", Journal of Acoustical Society of America, 1993, Vol 94, pp. 944-953

[11] Sullivan C., Kline R.A., and Mignogna R B "Acoustic tomographic reconstruction of fiber angle in orthographic composite materials", Progress in Quantitative Nondestructive Evaluation, 1998

[12] Rathoie S K , Munshi P , and Kishore N N "A new tomographic reconstruction method for anisotropic materials", 2003

[13] Subbarao P V , Munshi P , and Muralidhar K "Performance of iterative tomographic algorithms applied to nondestructive evaluation with limited data", NDT & E International, 1997, Vol 30, No 6, pp 359-370

[14] Mohd Farhan Manzoor "Ultrasonic tomography of Perspex/polystyrene composites", *M Tech Thesis*, July 1999, Nuclear Engineering and Technology Programme, Indian Institute of Technology, Kanpur

[15] Degtyar A D , and Rokhlin S I "Comparison of elastic constant determination in anisotropic materials from ultrasonic group and phase velocity data", Journal of Acoustical Society of America, 1997, Vol 102, pp 3458-3466

[16] Castagnede B , Jenkins J T , and Wolfgang Sachse "Optimal determination of the elastic constants of composite materials from ultrasonic wave speed measurements", Journal of Applied Physics, 1990, Vol 67, pp 2753-2761

[17] Reverdy F , and Audoin B "Elastic constant determination of anisotropic materials from phase velocities of acoustic waves generated and detected by lasers", Journal of Acoustical Society of America, 2001, Vol 109, pp 1965-1972

[18] Deschamps M , and Bescond C "Numerical method to recover the elastic constants from ultrasound group velocities", Ultrasonic, 1995, Vol 33, pp 205-211

[19] Spies M "Elastic waves in homogeneous and layered transversely isotropic media Plane waves and Gaussian wave packets A general approach", Journal of Acoustical Society of America, 1994, Vol 95, pp 1748-1760

[20] Rudzki M P "On apllication of Fermat's principle to anisotropic media",The society of Exploration Geophysicists,2000

SIMPLE ART PROGRAM USING MATLAB

```
% art z is convergence factor
% s is 30*30 slowness matrix
% err is  stopping criterion
% diff is difference between projection and calculated data
% y is number of iterations
diff=0,z=0 001,err=1 0,y=0,
s=ones(30,30),s=0 21*s,
s0=s,
% for o deg
while(err>=0 1),
s0=s,
fid=fopen('dataa0 txt','rt'),
a=fscanf(fid,'%f'),i=1,
while(i<=30),
sum=0,
for j=1 1 30,
sum=s(i,j)*1+sum,
end
diff=a(i)-sum,
for j=1 1 30,
s(i,j)=s(i,j) + z*1*(diff/30 0),
end
i=i+1,
end
fclose(fid),
% for 90 deg
fidl=fopen('data90 txt','r'),
a=fscanf(fidl,'%f'),
diff=0,j=1,
while(j<=30),
sum=0,
for i=1 1 30,
sum=1*s(i,j)+sum,
end
diff=a(j)-sum,
for i=1 1 30,
s(i,j)=s(i,j) +z*1*(diff/30 0),
end
j=j+1,
end
fclose(fidl),
```

```matlab
% for 45 and 135 deg
fidl=fopen('data45 txt','r'),
a=fscanf(fidl,'%f'),
diff=0,diff1=0,
for k=1 1 30,
i=k, sum=0,w=0,sum1=0,
for j=1 1 k,
sum=sum+0 707*s(i,j),sum1=sum1+0 707*s(31-i,j),
w=w+0 707,
if i>1
i=i-1,
sum=sum+0 707*s(i,j),sum1=sum1+0 707*s(31-i,j),
w=w+0 707,
end
end
diff=a(k)-sum,
diff1=a(k)-sum1,
i=k,
for j=1 1 k,
s(i,j)=s(i,j) +z*0 707*diff/w,
s(31-i,j)=s(31-i,j)+z*0 707*diff1/w,
if i>1
i=i-1,
s(i,j)=s(i,j)+z*0 707*diff/w,
s(31-i,j)=s(31-i,j)+z*0 707*diff1/w,
end
end

end
for k=1 1·30,
j=k, sum=0,w=0,sum1=0,
for i=30 -1·k,
sum=sum+0 707*s(i,j),
sum1=sum1+0 707*s(31-i,j),
w=w+0 707,
if j<30
j=j+1,
sum=sum+0 707*s(i,j),
sum1=sum1+0 707*s(31-i,j),
w=w+0 707,
end
end

diff=a(k+30)-sum,
diff1=a(k+30)-sum1,
j=k,
```

```
for i=30 -1 k,
s(i,j)=s(i,j)+z*0 707*diff/w,
s(31-i,j)=s(31-i,j)+z*0 707*diff1/w,

if j<30
j=j+1,
s(i,j)=s(i,j)+z*0 707*diff/w,
s(31-i,j)=s(31-i,j)+z*0 707*diff1/w,
end
end
end
eir=abs((s0-s)/(s)*100),
y=y+1,
end
% change of units to m/sec
s=s*0 001,
% tomographic image generation
r=1 1 30,
z=s,
[x,y]=meshgrid(r,r),
colormap(hsv),
pcolor(x,y,z),
rotate3d on,
view(3),
grid,
shading interp,
colorbar,
```

A 148394